Tomas Bata University in Zlín
Faculty of Technology

Fabrication of flexible supercapacitors with high electrochemical performance

Výroba flexibilního superkondenzátoru s vysokým elektrochemickým výkonem

Author: **Haojie Fei**

Study Programme: Chemistry and Materials Technology P 2808

Study Course: Technology of Macromolecular Compounds 2808V006

Supervisor: Prof. Petr Saha

Consultants: Assoc. Prof. Nabanita Saha and Ing. Robert Moučka, PhD

Zlín, 2017

Full-text of the doctoral thesis is available in the Library of TBU in Zlín.

Contents

Abstract

Flexible supercapacitors (SCs) are one kind of promising energy storage device for portable electronics. To gain a SC with high flexibility and electrochemical performance, such as high energy density, power density and cycling stability has drawn massive attention. However, to achieve this goal, there are challenges in the preparation of flexible electrodes and solid-sate electrolyte as well as the design and fabrication of flexible SCs. This doctoral thesis work is focused on the fabrication of flexible SCs with high electrochemical performance based on reduced graphene oxide (RGO) hydrogel.

This doctoral thesis has mainly been divided into two parts, the **theoretical part** (**Chapter 2 and 3**) and **research part (Chapter 5 and 6)**. At first, the thesis theoretically describes about the following points: (i) general properties of SCs and (ii) general information about the flexible SCs. At the former point, the advantage of SCs compared to the conventional capacitors and batteries is explained through the traditional electrochemical double-layer capacitors (EDLCs) following the capacitor principles (**Chapter 2.1 and 2.2**). There are *two* popular ways to increase the energy density of SCs: the use of *pseudo-capacitive materials* (**Chapter 2.3**) and the development of *asymmetric configuration* (**Chapter 2.4**) are both described. The importance of structural design of active electrode materials and conductive additives on electrochemical performance are also highlighted. Further, the measurements which are used to evaluate the electrochemical performance of electrodes such as cyclic voltammetry (CV), galvanostatic charge/discharge (GCD) and electrochemical impedance spectroscopy (EIS) are illustrated to mention their basic principles (**Chapter 2.5**). At the later point of flexible SCs, general information of the fabrication of flexible SCs has been introduced (**Chapter 3**). The mechanical theory of the film-on-substrate structure, regarded as the base of the fabrication of flexible electronics, is analysed, where three most important factors: (1) the thickness, (2) the flexible substrate and (3) mechanical neutral plane are emphasized (**Chapter 3.1**). Further, two widely used construction structures: (a) sandwich-type structure and (b) planar configuration are briefly introduced and compared (**Chapter 3.2**). The roles of RGO based flexible electrodes and gel/hydrogel electrolytes in flexible SCs are summarized. Their advantages and disadvantages of RGO hydrogel electrode are also discussed (**Chapter 3.3 and 3.4**).

The research part has been divided into two sections, as "**Experimental, (Chapter 5)**" and "**Results and discussion (Chapter 6)**". Firstly, the stable colloidal suspensions of RGO and MnO_2 were prepared. Based on these two colloidal suspensions, two RGO hydrogel composite films with redox-active materials, PANI and MnO_2, were prepared, respectively. To improve the

flexibility of the assembled SCs, two strategies, a free-movement configuration and the reduction of the thickness of entire devices were applied. Beside these, suitable gel electrolytes were prepared for the two constructional strategies. Finally, two flexible SCs were fabricated and characterized subsequently. In addition, for the study of hydrogel electrolyte, a mechanically strong hydrogel electrolyte was prepared and characterized.

Therefore, the study has been carried out with three directions and the results have been presented in three different sections, shown as **1) Chapter 6.1** *"Polyaniline/reduced graphene oxide hydrogel film with attached graphite current collector for flexible SCs"*, **2) Chapter 6.2** *"A highly flexible asymmetric SC using two dimensional nanomaterials and a bacterial cellulose filled neutral gel electrolyte"*, and **3) Chapter 6.2** *"In-situ preparation of bacterial cellulose reinforced hydrogel electrolyte for flexible SCs"*

Key words: *flexible supercapacitor, reduced graphene oxide, pseudo-capacitive material, hydrogel electrolyte*

1. INTRODUCTION

Recently, flexible electronics have drawn profound interrerest.[1-3] A great deal of achievement has been done in this field such as flexible organic light emitting diode (OLED) displays[4], electronic skins[5] and curved smart phones. However, one of their limits is the construction of flexible and deformable energy storage devices as their supplying power source.[6-8] These energy devices are required to keep high energy and power deliverability under continuous mechanical deformation for long cycles.[9]

Electrochemical capacitors (ECs) are also known as SCs, which are one of the most promising candidates for energy storage devices because of their extremely long cycle life (> 100000 cycles), fast charge/discharge, high power density (> 10 kW kg^{-1}) and simple structures.[10-12] ECs store energy using either ion adsorption (electrochemical double layer capacitors, EDLCs) or fast surface redox reactions (pseudo-capacitors). Recently, by decorating nano-sized pseudo-capacitive materials on high specific surface area (SSA) materials, pseudo-capacitors can achieve much higher energy density than EDCLs and reduce the suffering from their lack of stability during cycling.[13, 14] Thus they can complement or replace batteries in electrical energy storage as well as other area such as harvesting application.[15] However, conventional ECs are too heavy, thick and bulky to match flexibility requirements.

Therefore, to gain electrodes with robust mechanical flexibility, high energy density, power density and excellent cycling stability is the key to construct the

flexible energy devices. Reduced graphene oxide (RGO) is an ideal material for flexible electrodes due to its two-dimensional structure, high SSA and electric conductivity, as well as their low-cost, partial functionalization, compared to graphene.[16, 17] Thus, RGO films have been extensively studied as flexible electrodes. However, the aggregation and restacking of individual graphene nanosheets in these films reduce their specific surface area and re-wettability to electrolyte, resulting in blocking the diffusion of ions and decreasing the electrochemical performance.[18] RGO hydrogel films with a wet state have recently drawn massive attention because of their highly porous structure.[19]

On the other hand, the combination of flexible electrodes with compatible electrolytes and separators in the integral design and assembly of devices are important as well. A conventional flexible SC often consists of two flexible electrodes with current collectors separated by aqueous gel electrolyte. Since this classic sandwich-type flexible SC is constructed by piling up these components layer-by-layer, the large thickness of final SC device extremely hinders the flexibility. Therefore, optimizing the structural design of flexible SCs is required.[20]

This doctoral work is focused on the fabrication of flexible SCs with high electrochemical performance. To this end, flexible electrodes based on RGO hydrogel films modified by pseudo-active materials such as polyaniline (PANI) and manganese dioxide (MnO_2) have been prepared. Suitable gel electrolytes were prepared at the point of view to match the construction and electrochemical performance of flexible SCs. Finally, the construction of flexible SC was designed and investigated accordingly. The design of flexible SC is studied during the fabrication.

2. GENERAL PROPERTIES OF ELECTROCHEMICAL CAPACITORS

2.1 Principles of Capacitor

A capacitor is a passive component that stores energy in an electrostatic field. It is composed of two parallel electrodes (plates) separated by a dielectric. When applying a potential difference between these two electrodes, positive and negative charges migrate toward the surface of opposite polarized electrodes to be in a charged state. Once this charged capacitor is connected in a circuit, it can act as a voltage source for a short period.[21] As the following Equation (1), its capacitance (C) is the ratio of the electric charges stored in each electrode (Q) to the potential difference between them (V).

$$C = Q/V \qquad\qquad (1)$$

For a typical parallel plate capacitor, C is proportional to the area (A) of each electrode and the permittivity (ε) of the dielectric and inversely proportional to the distance (d) between the two electrodes, expressed as:

$$C = \varepsilon_0 \varepsilon_r A / d \qquad (2)$$

where ε_0 stands for the permittivity of free space and ε_r represents the dielectric constant (or relative permittivity) of the material between two plates. Therefore, the three main factors that determine the capacitance of a capacitor are (i) plate area, (ii) separation distance between two electrodes, (iii) properties of the dielectric used.

Two primary attributes of a capacitor are its energy and power density (specific energy or power), both of which can be expressed as a quantity per unit weight or per unit volume or unit area. The energy E (J) is directly proportional to its capacitance and the square of the potential difference (V) between two electrodes:

$$E = 1/2\, CV^2 \qquad (3)$$

$$P = E/t \qquad (4)$$

In general, average power (P) is the rate of energy delivery per unit time (t) as the above Equation (4). The power for a capacitor is usually measured at the matched impedance[22] which corresponds to the maximum power $P_{max.}$, expressed as

$$P_{max.} = V^2 / 4ESR \qquad (5)$$

The internal resistance of a capacitor includes the resistances of the components within a capacitor such as the electrode materials, current collectors, dielectric or electrolyte and separators.

2.2 Electrochemical double-layer capacitors

EDLCs store charge electrostatically by reversible ion adsorption occurring at the electrode/electrolyte interface. In the charged state, charges are separated and form a structure called "double layer" at the interface.[10] The electrodes of EDLCs have much higher effective surface area (A) and thinner dielectric in "double layer" (d), it results in a significant increase of both capacitance and energy than those of regular capacitors (Equation (2)). Moreover, because of the electrostatic charge storage mechanism, the series resistance of EDLCs does not contain any charge-transfer resistance, which is much lower than that of batteries at the cell level. Rapid ion adsorption/de-adsorption and low series resistance allow EDLCs very fast energy uptake and delivery, which explains their higher power density compared to that of batteries. In addition, due to the absence of faradic reactions, EDLCs can sustain millions of cycles whereas batteries survive a few thousand at best.[23]

The key to achieve high capacitance by electrostatic charge storage is to use those electrode materials with high SSA and electric conductivity. However, in reality, the relationship between specific capacitance and SSA does not follow a

linear trend. The capacitance increase was limited even for most of highly porous samples.

2.3 Redox-active materials to increase capacitance

Therefore, metal oxides such as MnO_2 and conducting polymers have been used in ECs, since these materials utilize fast and reversible redox reactions at their surface.[24] It represents a different kind of capacitance contribution to double-layer capacitance called pseudo-capacitance. This kind of ECs is usually called pseudo-capacitors, which posse higher energy density than EDLCs. But because redox reactions are used, like batteries, they often suffer from weakness of short cycling stability.

Since the reactions occurs only on or close to the interface of electrode and electrolyte, the low surface area of conventional pseudo-capacitive materials and slow ion diffusion in their bulk electrode highly reduce the interface for these reactions. In addition, the low electric conductivity of most pseudo-capacitive material hinders the transfer of electrons within the electrodes as well. These not only decrease their specific capacitance, consequently energy density but also reduce the power density. Thus, to achieve high-energy and high-power pseudo-capacitors, it is necessary to facilitate both the ionic and electronic currents within the electrodes by optimizing the design of nanostructured pseudo-capacitive materials on high SSA and electric conductive scaffold.[25]
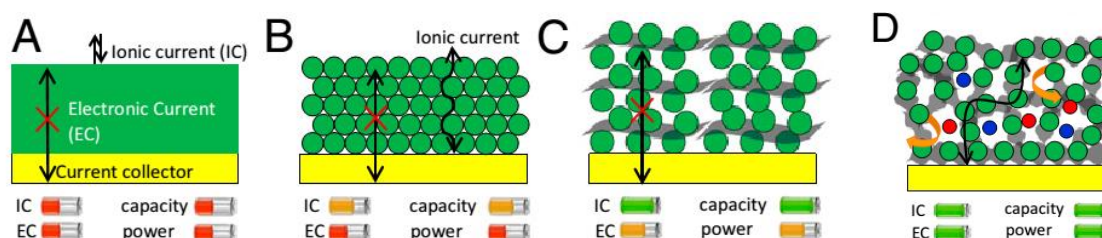

Figure 2-1 Rational design of supercapacitor electrodes with high energy and high power. Improving the ionic current (IC) and electronic current (EC) within the electrode is a key. Different approaches have been explored including (A) compact thick films of pseudo capacitive materials; (B) nanostructured pseudo capacitive material films; (C) addition of conductive materials to the nanostructured pseudo capacitive materials; and (D) recent approach of growing nanostructured pseudo capacitive material on 3D interconnected networks with high surface area and high electronic conductivity.[25]

As shown in Figure 2-1A, a layer of pseudo-capacitive materials is placed on the current collector. Only the top layer is exposed to the electrolyte solution. Therefore, nanostructured materials have been widely studied in the literatures. The porous structure of these electrodes increases the exposed area of active material (Figure 2-1B). This kind of system can exhibit higher energy density at very low currents, but it suffers from low power density. To improve the

electrical conductivity of entire electrode, conductive additives have been introduced into nanostructured electrodes. However, the electronic charge carriers must move through small interparticle contact area, resulting in poor electron transport from the electrode material to the current collector (Figure 2-1C). An ideal electrode would be obtained by growing 2D nanostructured redox-active materials onto a 3D interconnected macro-porous framework with high electrical conductivity and high surface area (Figure 2-1D). In such structure, both of high ionic current (IC) and electronic current (EC) can be obtained.[25]

Moreover, because ECs are power devices, their internal resistance must be kept low. Particular attention must be paid to the contact impedance between the active film and the current collector. Surface treatments of current collectors or the design of nanostructured current collectors are of great interest.[26]

2.4 Asymmetric (hybrid) systems to achieve high energy density

The maximum energy density ($E_{max.}$) is expressed as

$$E_{max.} = 1/2\, C U_{max.}^{2} \qquad (6)$$

and is proportional to the square of the maximum operating voltage ($U_{max.}$) of the cell, which is determined on the materials used for the electrode and electrolyte. For instance, EDLCs, porous carbon is used as the electrode material. In aqueous electrolytes, $U_{max.}$ is about 1 V, while in organic electrolytes U_{max} is in the range of 3-3.5 V. Herein, the operating voltage is determined by the electrolyte's stability window. Despite the higher capacitance (C) of carbon materials in aqueous electrolyte, the organic electrolyte is preferred because the EDLC in organic electrolytes obtains a higher energy density of 5.7 Wh kg^{-1} compared to 1.7 Wh kg^{-1} in aqueous electrolytes, benefiting from the square of larger U_{max}.[27] This superiority explains the reason that most commercial carbon/carbon based devices use organic electrolytes.

However, aqueous electrolytes possess a great amount of advantages such as their small ionic radius and high ionic conductivity, which are helpful to make their ECs achieve high specific capacitance and power density. In addition, aqueous electrolyte based ECs can be fabricated in moderate atmosphere conditions, while organic ones need strict processes and condition to keep ultra-pure. Another concern is electrothermal safety which is one of the major points now addressed by ECs manufacturers. Due to low resistivity, aqueous-based devices generate less heat than organic-based. It is significant especially when high currents and fast cycling rates are used.

The rapid development of electrode materials, especially these exhibiting faradaic or pseudo-capacitance with high-rate charge/discharge characteristics now enables a new class of ECs.[28] In these ECs, two distinct electrodes are paired in an asymmetric configuration, whereas a "pseudocapacitive" (MnO_2, Figure 2-2b) material is the positive electrode and a high surface-area carbon is

the negative electrode (Figure 2-2b). In such configuration, the high overpotentials for H_2 and O_2 evolution at the carbon-based negative electrode and pseudocapacitive positive electrode, respectively, extend the limit of potential window of aqueous electrolytes, resulting in significantly higher specific energy than for symmetric aqueous-based ECs. [28]
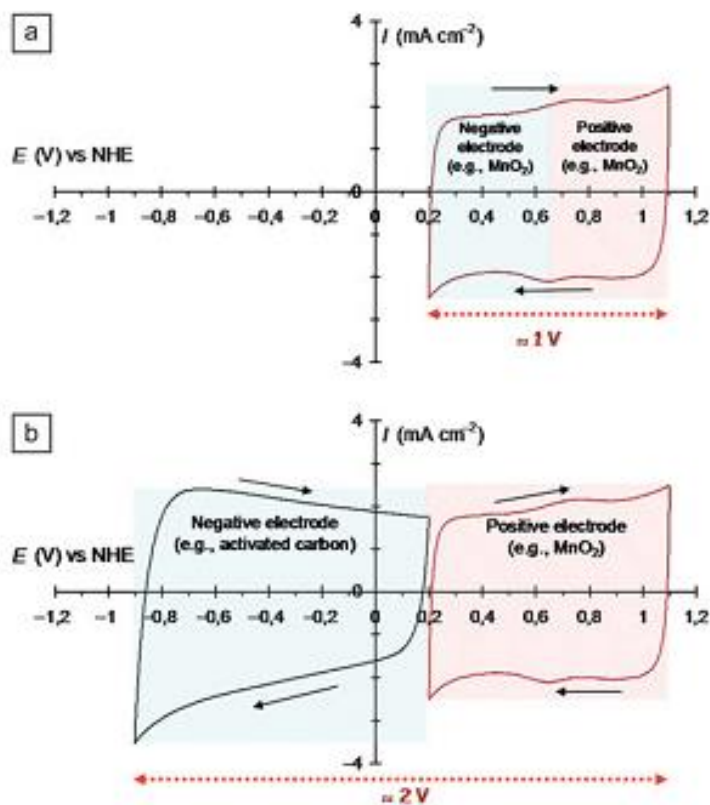

Figure 2-2 Schematic representation of cyclic voltammograms for three different configurations of aqueous-based ECs in which areas shaded in red and blue represent the potential window of the positive and negative electrode, respectively for (a) symmetric MnO₂//MnO₂ EC with α-MnO₂ electrodes in 0.5 M K₂SO₄; (b) asymmetric activated carbon//MnO₂ EC in 0.5 M K₂SO₄. [28]

To sufficiently utilize the electrochemically stable potential window of each electrode when their capacitor is charged, the weight ratio of the electrodes must be optimized, following the principle that the amount of charge, Q (C), stored in each of the positive and negative electrodes must be the same, and can be expressed by the following Equation (9) and (10):

$$Q = C_{sp+} \cdot w_+ \cdot \Delta U_+ = C_{sp-} \cdot w_- \cdot |\Delta U_-| \qquad (7)$$

$$U = \Delta U_+ + |\Delta U_-| \qquad (8)$$

where w_+ and w_- (g) represent the weight, C_{SP+} and C_{SP-} stand for the specific gravimetric capacitance, and ΔU_+ (V) and ΔU_- (V) are the potential window of the positive and negative electrodes, respectively. U is the operation voltage of the optimized capacitor. [29]

2.5 Electrochemical characterization

The electrochemical performance of ECs is measured by an electrochemical workstation. There are two test fixture configurations for the electrochemical cell, two-electrode and three-electrode configurations. For a two-electrode cell, the voltage measured (or controlled) is the cell voltage since the counter electrode (CE) and the reference electrode (RE) are shorted. For a three-electrode cell, a RE electrode is added, which exhibits a constant potential over a large range of currents. In this way, the voltage of working electrode (WE) is able to be accurately measured (or controlled).[30] Three most used electrochemical methods are cyclic voltammetry (CV), galvanostatic charge/discharge (GCD) and electrochemical impedance spectroscopy (EIS).

3. FLEXIBLE SUPERCAPACITORS

3.1 Mechanical theory of the film-on-substrate structure

Most flexible SCs mean that they are bendable. To fabricate high bendable electrodes which can properly work under a large degree of bending is the key for flexible SC devices. To this end, the mechanical analysis of electrode materials on flexible substrates is crucial and regarded as the theoretical basis for the design and implementation of flexible SCs.
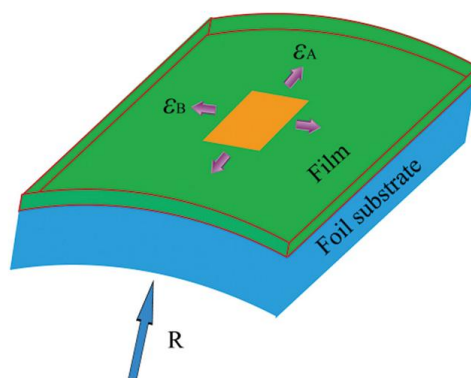

Figure 3-1 A multilayer film structure bending into a cylindrical roll.[12]

Figure 3-1 illustrates a bent film deposited on a compliant substrate (a multilayer film structure). It is the same structure as the conventional electrodes where the active material deposited on flexible substrates or metal current collectors.[12] As can be seen, the inner surface is compressed, while the outer surface is tensed. Strain in the film is mainly caused by an external bending moment. When the deposited film and the compliant substrate have the same Young's modulus, the strain in the top surface (ε_{top}) is as follows: [31]

$$\varepsilon_{top} = (d_f + d_s)/2R \qquad (9)$$

where the thickness and Young's moduli of the deposited film and the substrate are d_f and d_s, Y_f and Y_s, respectively. R is the bending radius. When the film and the substrate have different moduli ($Y_f > Y_s$), the neutral plane moves toward the more rigid film. (The neutral plane is a surface within film, where the material is not under stress, either compressive or tensile.) and the ε_{top} is given by

$$\varepsilon_{top} = \left(\frac{d_f+d_s}{2R}\right)\frac{(1+2\eta+\chi\eta^2)}{(1+\eta)(1+\chi\eta)}$$ (10)

where $\eta = d_f/d_s$ and $\chi = Y_f/Y_s$.

Importance of Thickness

According to Equation (12), the critical bending radius (R) scales linearly with the total thickness ($d_f + d_s$). Recently, lots of nanomaterials such as CNTs, graphene, nanowires and other nanosheets have attracted wide interest, owing to their high mechanical flexibility that originates from interconnected structures when they are stacked layer-by-layer to form a thin film. However, in order to obtain a higher specific capacitance upon the area, the deposited electrode materials have to be enhanced, resulting in the increase of the thickness. Large thickness leads to a large strain at the top of the deposited film. Even the film does not be fractured due to its large Young's moduli; it tends to be peeled off from the substrate. In this case, to adjust the ratio between Young's moduli of the film and substrate and to enhance the elongation of the film are important.

Use of flexible substrates

When the Young's moduli of the flexible substrate is much smaller than that of the active materials deposited film, the mechanical neutral plane moves toward to the deposited film, resulting in decreasing the stress.[32, 33] Thus, recently, more flexible substrates such as various polymers, cellulose papers, CNT films and graphene films have been widely used to support active materials and buffer built-in stress during bending. However, if substrates are too thin and soft, they can be easily stretched, hardly to protect the electrode film from the stretch force.

Effect of mechanical neutral plane

Another deduction from the above Equations (12) and (13) is that the strain in a film can be further reduced if the film is sandwiched between an encapsulation and a substrate layer with a suitable Young's modulus Y_e and thickness d_e.[12] When $Y_s d_s^2 = Y_e d_e^2$, the rigid film itself acts as the neutral plane.[12, 32] In this case, bending does not add any strain to the film, and the whole structure can be bent to an extremely small radius.

From the above analysis, three possible strategies to obtain bendable SCs are as follows: 1) Using nanostructured materials with a small thickness to fabricate free-standing film electrodes; 2) Depositing nanostructured materials onto

flexible substrates to further enhance the bendability of the electrodes; 3) Adding an encapsulation layer to tune the position of the neutral plane to the active material film.[12]

3.2 Structural design and optimization of flexible SCs

The most common structure for flexible SC is sandwich-type SC, as can been seen in Figure 3-2 (left). This type SC is constructed by layer-by-layer piling the electrodes, electrolyte (separator) and current collectors, which is a simple fabrication method. It is the popular fabrication method for free-standing electrode films with a large scale up to several centimeters. The deposition of the active electrode materials is usually larger than the planar configuration, resulting in a higher areal capacitance. To this end, it requires the free-standing electrode to obtain much strong mechanical properties.
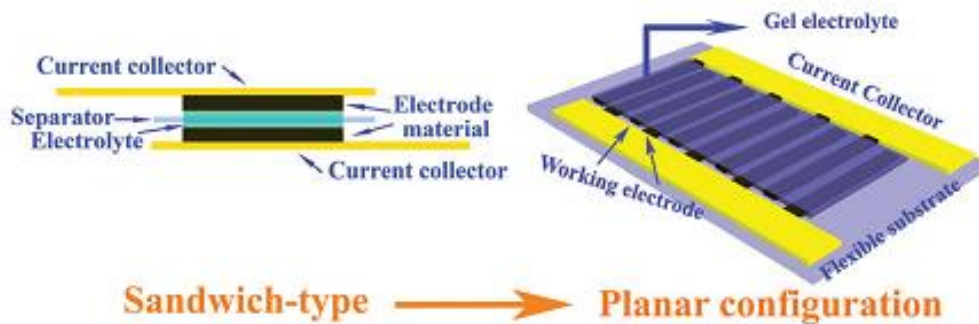

Figure 3-2 Schematic comparison of the sandwich-type supercapacitor (left) and planar supercapacitor (right).[20]
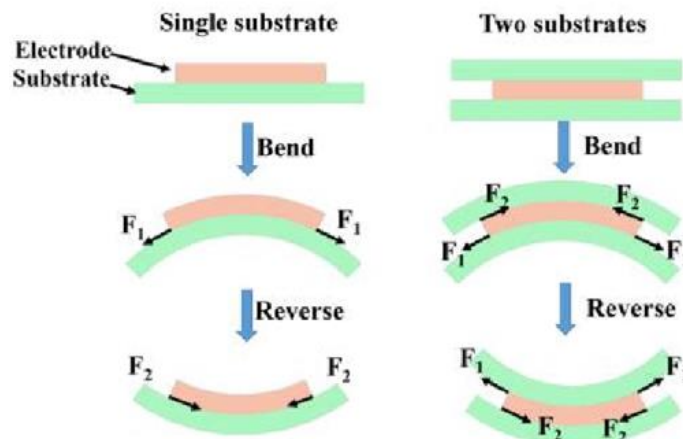
Figure 3-3 The distribution of stretching forces in the single-substrate and two-substrate devices at the bent state.[34]

On the other hand, as we know, the conductivity of the electrode is generally too low to serve itself as the current collector. Several reports have demonstrated that their electrodes can be the active materials as well as the current collector. But the scale of the prototypes is limited and the internal resistances are large.

Thus, flexible current collectors have to be paid more attention in the sandwich-type fabrication of flexible SCs. Based on this point, the interactions between the electrode film and the flexible current collector and their behaviors during the bending also are worthy to study. Another challenge of flexible current collectors is the corrosion of metals in aqueous electrolytes. The use of noble metals reduces the advantage of low-cost of aqueous electrolyte based supercapaciotrs.

The most disadvantage of this structure is that the entire device is thick, which reduces its flexibility as be discussed in section 3.1 above. Even worse, the deformation behavior of this sandwich structure during the bending is more complicated due to the soft layer of gel/hydrogel electrolyte in the middle.[34] As shown in Figure 3-3, shear forces occurs and revers the orientation during the cycle of bending.

3.3 RGO hydrogel based flexible electrode

Flexible electrodes are the key component in flexible SCs. Owing to the electrodes of commercial SCs are usually prepared by slurries that consist of active material (powder form), polymer binders and conductive additives using casting method. The obtained electrodes generally cannot meet the requirement of flexibility, when the thickness increases. Therefore, a new class of mechanically flexible electrodes without binder and conductive additives has been developed based on various materials such as activated carbon, carbon nanotubes, carbon fiber and graphene with novel configuration designs shown in Figure 3-4.
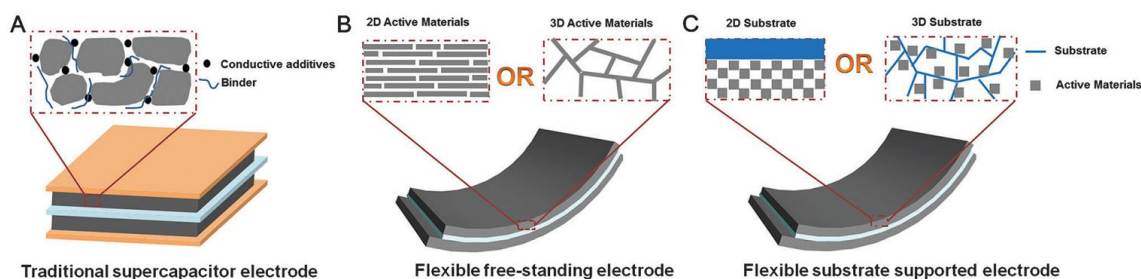

Figure 3-4 Schematic showing the structural difference between (A) conventional and (B, C) flexible electrodes in SCs.[9]

Among them, reduced graphene oxide (RGO) have been extensively studied as electrode materials for flexible electrodes due to their two-dimensional nanosheet structure, high specific surface area, and excellent flexibility, as well as their easy access, partial functionalization and low-cost, compared to graphene.[35] By various methods, RGO self-supporting films could be prepared with robust mechanical strength.[36] However, during the preparation, especially the drying process, aggregation and restacking of individual graphene nanosheets reduce the specific surface area of these obtained films and their re-wettability to electrolyte, resulting in blocking the diffusion of ions and

decreasing the electrochemical performance.[18] Thus, RGO hydrogel films with a wet state have recently drawn massive attention since their highly porous structure stores abundant electrolyte and provides continuous pathway for electrolyte ions.[37, 38]

However, due to the limited capacitance contribution of electrochemical double layer, the capacitance values of RGO hydrogel films are still lower compared to these of pseudocapacitors that involve Faradic reactions for storing the charge. In this case, pseudocapacitive materials such as transition metal oxides and conducting polymers are common to be employed into.[39, 40] On the other hand, the defects on graphene nanosheets caused by oxidation degrade their qualities, especially their electrical conductivity. In consequence, electronic transport in these films cannot meet the demand for devices, especially for these who have large-scale electrodes and intend to work at high current. Therefore, current collectors are still extremely necessary. Moreover, since the restacking of RGO nanosheets is reduced in RGO hydrogel, their mechanical property is lower than RGO free-standing films. Thus, the fabrication method or the structural design and optimization of flexible SCs are necessary to take into consideration.

3.4 Gel/hydrogel electrolyte

Due to the deformation of flexible SCs, the leakage of liquid electrolyte aggravates. Rather than improving the sealing technique, the use of solid state electrolyte is more practical. In case of aqueous electrolyte, the gel or hydrogel electrolyte are generally used.[41-43] Generally, the gel electrolyte is prepared by dissolving suitable polymers into aqueous electrolyte to form gels with high viscosity. However, these gels usually are just cross-linked by physical hydrogen bond, which can be broken down when the temperature increases. Hydrogel electrolyte is a hopeful candidate since it can hold enormous aqueous electrolyte, which makes sure that it has a similarly high ionic conductivity corresponding to the aqueous electrolyte, but remains in a quasi-solid state even at high temperature due to their chemical crosslinking.[44] Recently, material scientists are developing various polymer hydrogels as solid electrolytes for flexible SCs.[45, 46] Unfortunately, most of them are lack of mechanical property as they contain too much water. In addition, the hydrogel electrolyte is a form of membrane, which has a bad interaction between the electrodes and them. The adhesion of electrode and electrolyte can be easily destroyed, especially in the bend state of the flexible SCs. One of the strategies to solve this problem is to in situ polymerize the hydrogel electrolyte directly between two electrodes in presence of electrolyte solution and reinforcing materials. Two electrodes would be united as a whole and flexible SCs could be assembled.

4. AIMS OF DOCTORAL THESIS

This doctoral thesis is focused on the fabrication of flexible SCs with high electrochemical properties. To achieve this goal, the work has been divided into several parts.

1. Preparation of flexible electrode materials: (i) preparation of highly conductive and porous RGO hydrogel film, (ii) modification of RGO hydrogel film by pseudo capacitive materials such as PANI and MnO_2.

2. Preparation of gel/hydrogel electrolytes for the fabrication of flexible devices.

3. Design of flexible device according to the properties of obtained composite electrodes and gel/hydrogel electrolytes.

4. Fabrication of flexible device and investigation of its electrochemical performance and flexibility.

5. EXPERIMENTAL

5.1 Materials and samples preparation

Preparation of GO, RGO and MnO2 colliodal susuepensions

Graphite oxide was prepared by the oxidation of natural graphite flakes (325 mesh, Graphite Tyn) according to a modified Hummers' method.[47] RGO colloid was obtained by reducing GO dispersion with electrostatic stabilization.[36] A typical procedure was as follows: 6 mL of 3 mg/mL GO dispersion, 1 mL of ammonium hydroxide solution (30 ~ 32 wt. %) and 100 μL of hydrazine hydrate (50 ~ 60 wt. %) were added in a flask filled with 200 mL of deionized water. This mixture was then severely shaken. The RGO colloid was obtained by placing this flask in a water bath with temperature of 90 ^{o}C for 2 h.

MnO_2 colloidal suspension was prepared according to a previous literature.[48] Typical procedure was as follows: 12 mL 1 M tetramethylammonium hydroxide (TMAOH) and 2 mL 30 wt. % H_2O_2 were mixed and diluted to 40 mL by deionized water. Then, this mixed solution was poured to 10 mL 0.3 M $Mn(NO_3)_2$ under vigorous stirring and kept stirring for 12 h at room temperature. The resulting suspension was dialyzed in deionized water. Finally, the MnO_2 colloid was obtained by centrifuge to separate the precipitate.

Preparation of RGO/G, PANI/RGO/G and MnO2/RGO/G hydrogel films

RGO hydrogel films were prepared by vacuum filtration of RGO colloid. To obtain a graphite current collector on RGO/G, at the end of the filtration, the top of hydrogel films was rinsed by dilute ammonia water solution, and then 2 mL of 1mg/mL graphite suspension was added into until the filtration completed.

PANI/RGO/G hydrogel films were obtained by in-situ polymerization of aniline onto an RGO/G. A typical procedure was as follows: RGO/G filter cakes

were cut into rectangular pieces with a size of 1 cm × 2 cm. Two pieces of these films were immersed into 10 mL of 1.0 M HCl aqueous solution containing 90 μL of aniline monomer. The mixture was stored at 0 °C for 2 h. 10 mL of 1.0 M HCl aqueous solution containing 0.155 g ammonium persulfate (pre-cooled to 0 °C) was then poured into the above mixture. This mixture was left at 0 °C for another 24 h. The resulting films were immersed in HCl aqueous solution, ethanol, and deionized water subsequently. Finally, the films were compressed between two pieces of polyvinylidene fluoride (PVDF) filter membranes under 10 MPa. The schematic illustration of PANI/RGO/G hydrogel film formation

MnO$_2$/RGO hydrogels were prepared by vacuum filtration of mixed MnO$_2$/RGO colloid. The mixed suspension was obtained by mixing two pure colloids by a mass ratio of 50/50. A graphite current collector was deposited on these hydrogels by successive filtration of graphite flakes suspension. The desired flexible hydrogel electrodes were obtained by compressing these hydrogels between two pieces of PVDF filter membranes under 15 MPa.

Preparation of the BC modified PAAS-Na$_2$SO$_4$ gel electrolyte

Polyacrylic acid sodium salt (PAAS) gel was synthesized by the radical polymerization of acrylic acid in water. Typical procedure was as follows: 3.5 g acrylic acid was neutralized by NaOH in 8 mL deionized water. Then 1.95 g potassium persulfate (K$_2$S$_2$O$_8$) was added in this solution. The polymerization was conducted at 85 °C with stirring and in N$_2$ atmosphere to gain PAAS gel. Then, 20 g wet BC membrane was grinded into BC clusters and precipitated by a centrifuge with the speed of 8000 rpm (Rotina 380, Hettich). The BC precipitation and 3.98 g Na$_2$SO$_4$ were mixed with previous PAAS gel electrolyte to obtain BC/PAAS-Na$_2$SO$_4$ gel electrolyte.

Fabrication of flexible SC using PANI/RGO/G hydrogel films

The packing substrate (poly(dimethyl siloxane), (PDMS) of the device was prepared from SYLGARD ® 184 (Dow Corning Corporation). It represents a slide (thickness = 0.2 cm) with a cavity (2.5 cm long, 1.3 cm wide, 0.15 cm deep). Two prepared PANI/RGO/G films were put into the cavity, separated and surrounded by poly(vinyl alcohol)-H$_2$SO$_4$ (PVA-H$_2$SO$_4$) gel electrolyte (10 g PVA (M$_w$, ~ 145,000) dissolved in 90 g 1 M H$_2$SO$_4$ solution). Two titanium foils were placed on each edge of the films with an area of 1 cm × 0.5 cm. This part of the films was pre-dried on a hot plate for seconds at a temperature of about 80 °C and separated by Parafilm. The effective electrode area was 1 cm × 1.5 cm. Then a polyethylene terephthalate (PET) substrate was put on the top for sealing. Finally, the titanium foils were fixed by a clip.

Fabrication of the flexible SC using RGO/G and MnO$_2$/RGO/G hydrogel film

Compressed RGO/G and MnO₂/RGO/g hydrogel films were cut to a size of 3 cm × 1 cm with a tail of 1.25 cm × 0.3 cm for the connection with titanium foils. Each piece of RGO and MnO_2/RGO hydrogel films was placed on the polyethylene (PE) films (40 μm，thickness). Then, they were assembled face to face, separated by BC modified PAAS-Na_2SO_4 gel electrolyte with a traditional sandwich-type structure. Finally, they were compressed under 0.5 MPa between two flat plates to obtain the flexible SC device.

Preparation of hydrogel electrolytes

Procedure for the preparation of hydrogel electrolytes was as follows: 3.6 g acrylic acid was dissolved in 2.5 mL water and neutralized by 2.86 g KOH. Then, 1 g poly(ethylene glycol) diacrylate (PEGDA), 0.06 g $CaSO_4 \cdot H_2O$, 7.5 g BC suspension (0.2 wt. %) and 25.6 mg (Potassium persulfate) KPS was added into this solution. Finally, the obtained solution was dropped into 18.4 g sodium alginate (SA) solution (5 wt. %) under stirring. The mixture was casted into a mold and kept in the oven for 1 h at 80 °C. The gained hydrogel was immersed into 1 M $CaCl_2$ solution for 2 days and then in 2 M KCl for 1 day. SA crosslinked by $CaSO_4 \cdot H_2O$ was designated as "SA-$CaSO_4$", and crosslinked by $CaSO_4 \cdot H_2O$ and $CaCl_2$ was named as "SA-Ca".

5.2 Characterization

The morphology and structure of obtained nanomaterials and their composite films were characterized by Atomic force microscopy (AFM, Dimension Icon, Bruker), scanning electron microscopy (SEM, FEI Nova NanoSEM450), transmission electron microscopy (TEM, JEOL JEM-2100) and X-ray diffraction (XRD, Rigaku MiniFlex 600). The Raman spectra were obtained using a Raman spectrometer (Jobin-Yvon, LabRam HR). The Zeta potentials of MnO_2 and RGO in colloidal suspensions were measured by Zetasizer Nano ZS90 (Malvern). The rheology behavior of PAAS-Na_2SO_4 gel electrolyte was examed by the Rheometer MCR 502 (Anton-Paar). The resultant hydrogel was characterized by ATR-FTIR (Nicolet iS5). The compression test was conducted by Testometric MT350-5CT.

The electrochemical characterization was carried out by cyclic voltammetry (CV), galvanostatic charge-discharge test and electrochemical impedance spectroscopy (EIS) using Autolab PGSTAT128N (Metrohm, Netherlands). The electrochemical performance of the prepared hydrogel films was first investigated in a three-electrode system with an Ag/AgCl reference electrode and a Platinum counter electrode. The specific capacitance of the electrodes from CV profile (C_{sp}) was calculated using the following equation:

$$C_{sp} = \int I \, dU / 2vm\Delta U \qquad (21)$$

where I is the current, $\int I \, dU$ is the integration area for the CV curve, v is the scan rate, m is the mass of the active material, ΔU is the potential window, the

factor 2 corrects the fact that above integration area includes both the positive and negative scan. The measurement for assembled devices was carried out in a two-electrode system. The specific capacitance of each device was calculated from the galvanostaic curves at different current densities using the formula:

$$C_t = I\Delta t/m\Delta V \qquad (22)$$

where I is the discharge current, Δt stands for the discharge time, m is the total mass of active materials in both electrodes (without graphite current collectors), and ΔV is the voltage drop upon discharging (excluding IR_{drop}, the potential drop at the beginning of the discharge in charge-discharge profile). The areal capacitance (C_A) of each device was calculated by following equation:

$$C_A = C_t/A, \qquad (23)$$

where A is the footprint area of the electrodes. For the symmetric cells, the specific capacitance (C_{sc}) of one electrode was calculated following the equation:

$$C_{sc} = 4C_t \qquad (24)$$

Finally, the energy density (E) and power density (P) of each device was derived from the equation:

$$E = C_t\Delta V^2/2 \qquad (25)$$

$$P = E/\Delta t \qquad (26)$$

6. RESULTS AND DISCUSSION

6.1 Polyaniline/reduced graphene oxide hydrogel film with attached graphite current collector for flexible supercapacitors

In this paper, we report the fabrication and characterization of one flexible SC device based on PANI/RGO/G hydrogel films. A graphite current collector was directly deposited on the surface of an RGO hydrogel film and modified by PANI through a diluted in-situ polymerization. During the fabrication of the SC device, a special design of the device was adopted to solve the problem of weak mechanical properties of RGO hydrogel films. As a result, high electrochemical performance of the device has been achieved due to (i) the high diffusion of electrolyte ions in hydrogel films, (ii) the contribution of high pseudocapacitance of PANI, and (iii) the enhanced electron transport endowed by a graphite current collector. Moreover, owing to the special design, this device exhibits high flexibility. This study shows a promising possibility for the application of RGO hydrogel based films in flexible SCs.

In order to increase the electron transport in RGO hydrogel films, graphite flakes were deposited on one side of RGO hydrogels, serving as a current

collector after successive filtration of RGO dispersion and graphite suspension, as illustrated in Figure 6-1. After compressing RGO/G and PANI/RGO/G hydrogel films, graphite flakes are strongly attached to RGO matrix; it also improves their flexibility and mechanical properties. Figure 6-1 displays the digital images of the compressed RGO/G and PANI/RGO/G films. Both of them exhibit high flexibility.
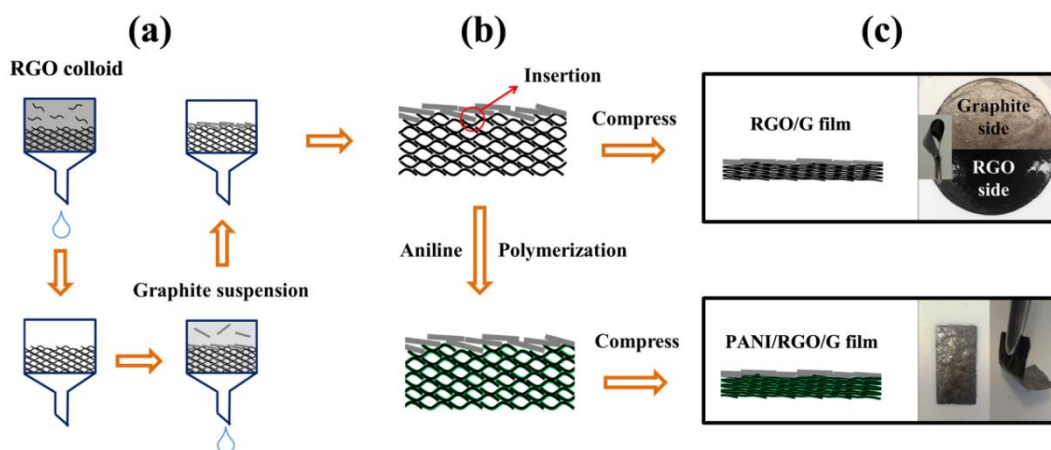

Figure 6-1 Schematic illustration of the preparation process. (a) Successive filtration of RGO colloid and graphite suspension to deposit graphite flakes on the surface of RGO hydrogel. (b) Insertion of graphite flakes and in-situ polymerization of aniline onto RGO. (c) Digital images of flexible RGO/G and PANI/RGO/G hydrogel films after compression.
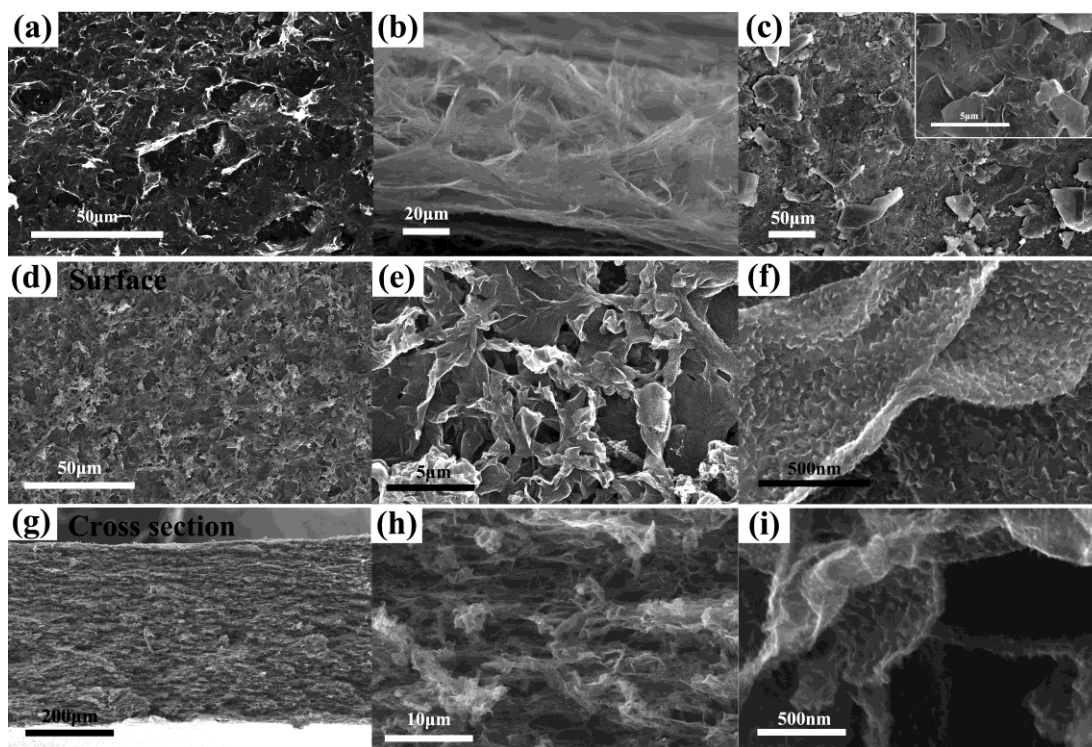

Figure 6-2 SEM images of the surface of RGO hydrogel from (a) top view and (b) side perspective, (c) the surface of graphite side of RGO/G film (inset image shows its high magnification image), (d) the surface of PANI/RGO hydrogel and (e, f) at high

magnification, (g) the cross-section of PANI/RGO hydrogel and (h, i) at high magnification.

RGO film exhibits porous structure, providing continuous ionic pathways across piled RGO layers (Figure 6-2a). Importantly, RGO flakes stand on the surface of a film, from the side perspective (Figure 6-2b). That is why graphite flakes can be embedded into the RGO film during the filtration and then held tightly after compression. Figure 6-2c obviously shows that small hard graphite flakes are embraced by soft RGO sheets. This makes this graphite current collector deformable along with the RGO film without splitting during bending. Figure 6-2e and 5-2f show that PANI nanoarrays grow on the surface of RGO nanosheets. Figure 6-2h demonstrates a layer-by-layer structure with a highly developed porous structure of PANI/RGO. Figure 6-2i confirms that PANI nanoarrays are present not only on the surface but also inside the hydrogel. This fine growth of PANI nanoarrays and their uniform distribution benefit from the interconnected channels within hydrogel as well as from the low concentration of aniline in the reaction media. A thin PANI layer (59 wt. % in PANI/RGO) deposited on RGO tends to endow the electrode with excellent electrochemical performance.[49]
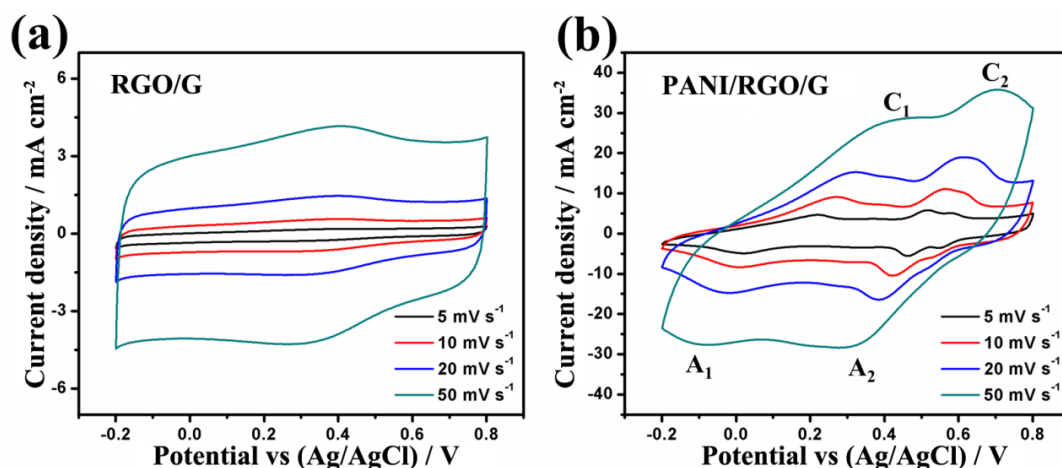

Figure 6-3 Cyclic voltammogram curves of (a) RGO/G and (b) PANI/RGO/G at various scan rates from 5 to 50 mV s^{-1} collected in a three-electrode system with an Ag/AgCl reference in 1 M H$_2$SO$_4$. Note that the y-scale in (a) is much smaller than (b).

The RGO/G and PANI/RGO/G were first analyzed by CV in a three-electrode system in 1 M H$_2$SO$_4$ with a potential window from –0.2 to 0.8 V *versus* Ag/AgCl. The CV curves show a remarkable difference between the electrochemical activities of RGO/G and PANI/RGO/G (Figure 6-3). Two pairs of redox peaks (C$_1$/A$_1$, C$_2$/A$_2$) from PANI/RGO/G indicate the presence of pseudocapacitive PANI (Figure 6-3b).[52] PANI/RGO/G exhibits a higher specific capacitance of 806 mF cm^{-2} (548 F g^{-1} excluding the mass of graphite current collector), compared to that of RGO/G (142 mF cm^{-2}, and 218 F g^{-1}) at a scan rate of 5 mV s^{-1}.
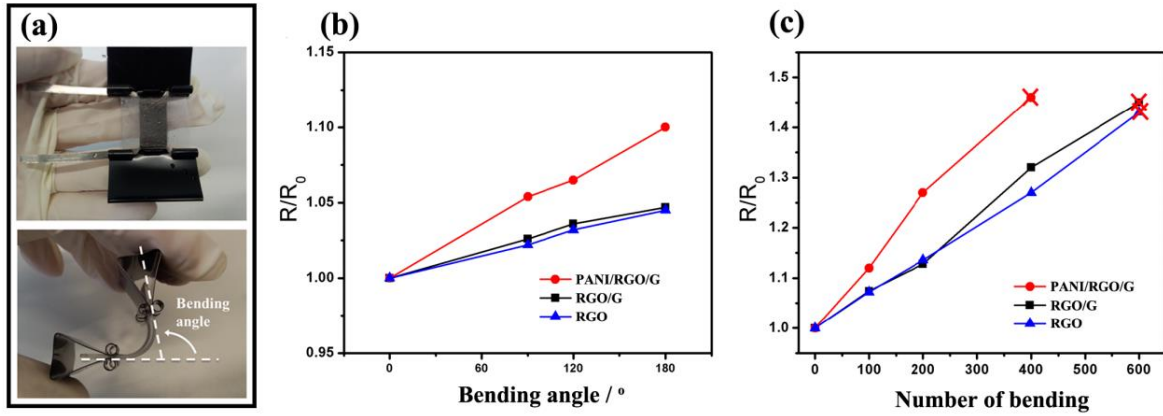
Figure 6-4(a) Image of one fixed set for bending ability test and the illustration of the bending angle. Normalized resistances of prepared hydrogel films after bending as a function of (b) the bending angle and (c) the number of bending (the red cross indicates when the fracture occurs).
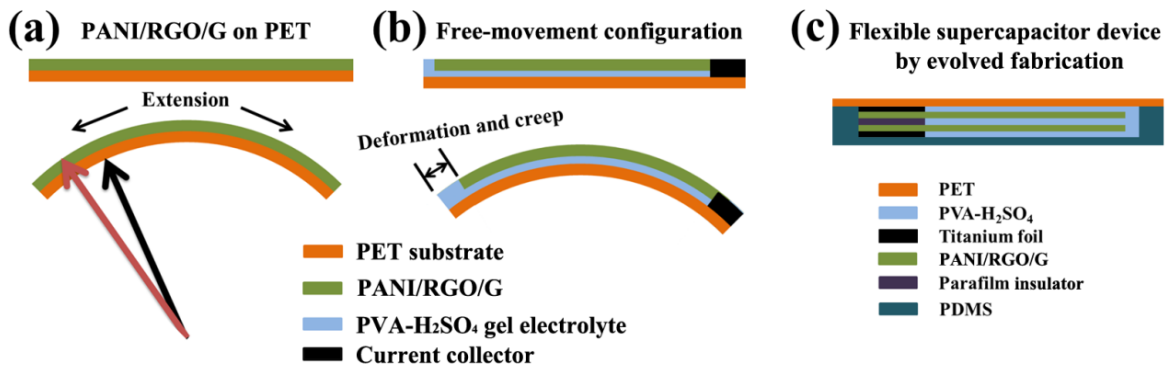

Figure 6-5 (a) Schematic diagram of PANI/RGO/G hydrogel film on a PET substrate and the different extensions upon the radius caused by bending. (b) Free-movement configuration and its mechanism to reduce the stress force during bending. (c) Illustration for constructing flexible supercapacitor devices using a free-movement configuration (cross section).

However, during the fabrication of flexible SCs, the prepared hydrogel films exhibit weak mechanical properties. The bending fixture and bending test results are demonstrated in Figure 6-4(a). Graphite current collector rarely decreases the bending ability of films, but the deposition of PANI does (Figure 6-4b). Importantly, the damage of each film deteriorates as the angle and the number of bending increase (Figure 6-4c). The structural design plays an important role in the flexibility of devices. Several strategies have been reported, such as using a planar configuration, reducing the thickness and optimizing the mechanical neutral plane.[12, 20, 53] Here, an alternative approach was demonstrated. The schematic diagram of SC fabrication is shown in Figure 6-5. As can been seen, when the multilayer of PANI/RGO/G and PET substrate gets bent, the lengths are getting different upon the radius from the center of concentric circles (Figure 6-5a). Thus, the top of PANI/RGO/G is stretched.[32] Since PANI/RGO/G hydrogel has low tensibility, it tends to be torn up. Therefore, a free-movement

configuration was adopted (Figure 6-5b). PANI/RGO/G and the PET substrate are separated by PVA-H_2SO_4 gel electrolyte, and only one side of PANI/RGO/G is provided with current collector. As a result, due to the large deformation and creep of gel electrolyte, PANI/RGO/G can freely move when bent, the stress applied to PANI/RGO/G from gel electrolyte is much lower than that from PET substrate. This free-movement configuration has been adopted to assemble a flexible SC device (Figure 6-5c).

Electrochemical performance of assembled flexible SC devices with various hydrogel films was subsequently characterized. Firstly the effect of a graphite current collector was studied. Figures 6-6a and 6-6b show the galvanostatic discharge profiles of PANI/RGO and PANI/RGO/G at various current densities. Each IR_{drop} of PANI/RGO/G is extremely lower than that of PANI/RGO for the corresponding current density. The IR_{drop} vs current densities are summarized in the inset graph in Figure 6-6b. Because of the contribution of PANI, PANI/RGO/G exhibits a much higher specific gravimetric capacitance (C_{sc}) of 409 F g^{-1} (478 F g^{-1}, excluding the mass of graphite current collector) at 2 mA cm^{-2}, compared to that of RGO/G (110 F g^{-1} and 152 F g^{-1}, respectively), and similar to that of PANI/RGO (457 F g^{-1}). The PANI/RGO/G device yields a gravimetric capacitance (C_t) of 120 F g^{-1} based on the total mass of two electrodes, and an areal specific capacitance of 352 mF cm^{-2} at 2 mA cm^{-2}, which is much higher than that of RGO/G (49 mF cm^{-2}). The PANI/RGO/G device displays good rate performance with only 11.9% capacitance loss when current density increases from 1 mA cm^{-2} to 10 mA cm^{-2}.

The CV profile of dry PANI/RGO/G (Figures 6-6c) is distorted and turns to be spindle-like as the scan rate increases (from 5 to 100 mV s^{-1}), while that of PANI/RGO/G hydrogel film (Figures 6-6c) exhibits much better retention. This is attributed to the high ion transport in the PANI/RGO/G. This is confirmed in Figure 6-6e, which shows the impedance curves of assembled devices with various films. The charge transfer resistance (R_{ct}) of PANI/RGO/G, extracted from the intercept of the low-frequency impedance spectrum with the real axis, is 3.5 Ω, which is almost the same as that of RGO/G but much lower than those of PANI/RGO and dry PANI/RGO/G. This indicates that the graphite current collector reduces the resistance of the films and that the interconnected porous structure of hydrogel films ensures fast ion diffusion.[25] Indeed, the fabricated device demonstrates a higher energy density of 27.8 μWh cm^{-2} (8.1 Wh kg^{-1}) and a larger power density of 3.5 mW cm^{-2} (1.0 kW kg^{-1}) compared to those of PANI/RGO (20.8 μWh cm^{-2} (6.5 Wh kg^{-1}) and 2.0 mW cm^{-2} (0.6 kW kg^{-1}), respectively (inset image in Figure 6-6f).
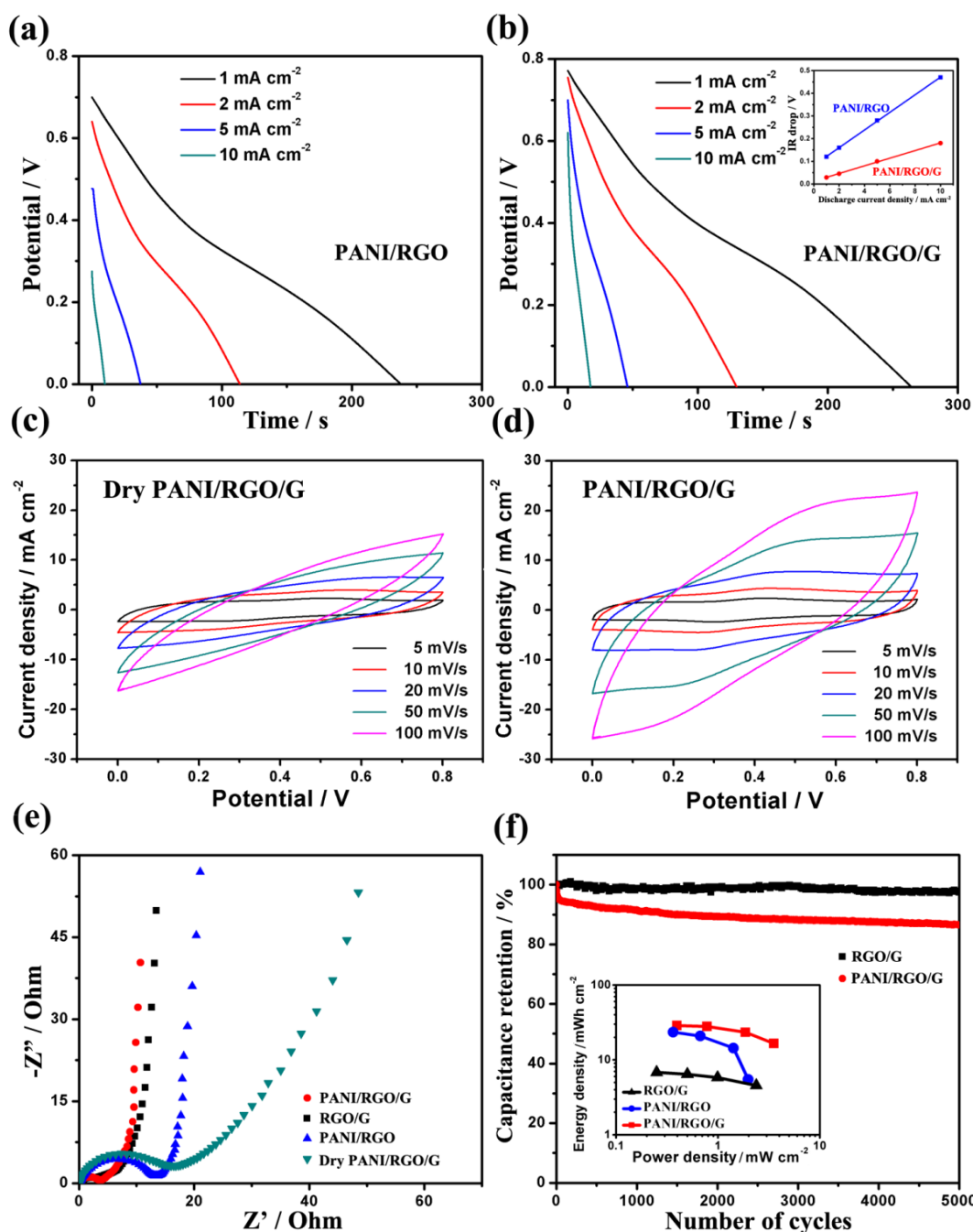
Figure 6-6 Electrochemical performance of symmetric flexible devices using various prepared films. Galvanostatic discharge curves of (a) PANI/RGO and (b) PANI/RGO/G devices at various current densities from 1 mA cm^{-2} to 10 mA cm^{-2}; inset graph shows the summary of their IR$_{drop}$ vs current densities. Cyclic voltammograms of (c) dry PANI/RGO/G and (d) PANI/RGO/G hydrogel film device at different scan rates from 5 mV s^{-1} to 100 mV s^{-1}. (e) Nyquist plots demonstrate the effect of graphite current collector and wet-state of the films on R$_{ct}$. (f) Cycling stability of RGO/G and PANI/RGO/G devices at a high current density of 5 mA cm^{-2} (inset image shows their areal energy densities vs average power densities).

Furthermore, unlike general PANI-based SCs, this device exhibits a good cycling stability, showing capacitance retention as high as ~86.5 % over 5000 cycles at a high current density of 5 mA cm^{-2} (Figure 6-6f).[55, 56]
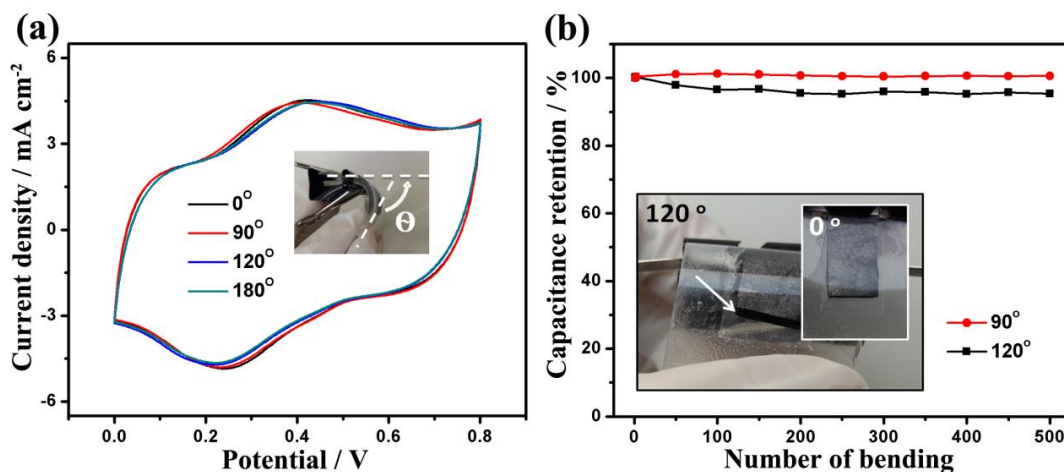

Figure 6-7 *Flexibility of PANI/RGO/G device using a free-movement configuration. (a) Cyclic voltammograms at various bending angles at 10 mV s^{-1}. (b) Capacitance retention after various bending cycles at angles of 90° and 120° (inset image shows the deformation of gel electrolyte).*

The flexibility of the fabricated device and its influence on the electrochemical performance were investigated further. Figure 6-7a shows that only a slight change can be observed on the CV curves, when the bending angle is from 90 ^{o} to 180 ^{o}. The capacitance retentions of the device after different numbers of bending are presented in Figure 6-7b. When the bending angle keeps at 90 ^{o}, the device has almost the same capacitance as the initial one even after 500 times of bending. The obtained results confirm the improved flexibility achieved by using a free-movement configuration. The inset digital image in Figure 6-7b shows that when the bending angle turns from 0 ^{o} to 120 ^{o}, the gel electrolyte is sheared by two parallel films on each side. The films keep their initial length, the elongation occurring in the gel electrolyte. Due to the high deformation and creep of the gel electrolyte, a slight shear force is applied to the hydrogel films.

Conclusions

This work has demonstrated about a flexible SC device with high electrochemical performance and improved flexibility by using PANI/RGO/G hydrogel films and a free-movement configuration. The modification of RGO/G hydrogel film by PANI results in an enhanced areal capacitance of 352 mF cm^{-2} (478 F g^{-1}) and energy density of 27.8 µWh cm^{-2} (8.1 Wh kg^{-1}) compared to those of RGO/G (49 mF cm^{-2}, 152 F g^{-1}) at a current density of 2 mA cm^{-2}. Moreover, a low-cost but efficient method was adopted to create a flexible current collector on RGO hydrogel film using graphite flakes. This graphite

current collector reduces the internal resistance of the device (R_{ct} = 3.5 Ω), which manifests itself in an enhanced power density up to 3.5 mW cm^{-2} (1.0 kW kg^{-1}) at a current density of 10 mA cm^{-2}. Moreover, this device also exhibits a good cycling stability (86.5 % retention after 5000 cycles) at a high current density of 5 mA cm^{-2}, as well as an improved flexibility, where its capacitance hardly changes after 500 cycles of bending at a bending angle of 90 ^{o}. Due to the free-movement configuration, PANI/RGO/G is suspended in gel electrolyte. The large deformation and creep of PVA-H$_2$SO$_4$ gel electrolyte deceases the applied stress from the PET substrate to PANI/RGO/G. This study shows a new approach to the application of mechanically weak film electrodes, especially RGO hydrogel based films, in flexible SCs.

6.2 A highly flexible asymmetric supercapacitor using two dimensional nanomaterials and a bacterial cellulose filled neutral gel electrolyte

In the present study, a flexible asymmetric SC device has been assembled using MnO$_2$/RGO (positive electrode) and RGO hydrogel films (negative electrode). A novel bacterial cellulose (BC) clusters filled polyacrylic acid sodium salt-Na$_2$SO$_4$ (BC/PAAS-Na$_2$SO$_4$) gel electrolyte was used to reduce the thickness of electrolyte layer, where BC cutlers filled in the gel can prevent from the contact of two electrodes during the compression. The assembled flexible cell exhibits high flexibility in sandwich-type construction, benefiting from the thin gel electrolyte layer as well as the use of 2D nanomaterials pilled flexible electrodes. It also displays good electrochemical performance due to the asymmetric configuration and high ionic diffusion in hydrogel electrodes. This device is very environmentally friendly, safe and low cost due to the appropriate selection of electrode materials and electrolyte.

In order to prepare RGO and MnO$_2$/RGO hydrogel films through the vacuum filtration, firstly, stable RGO and MnO$_2$/RGO colloidal suspensions have to be obtained. Figure 6-8a shows the photograph of RGO and MnO$_2$ colloidal suspensions and their mixture (MnO$_2$/RGO), respectively. They demonstrate the Tyndall effect, which indicates their colloidal behavior. However, their stability in time is considerably affected by pH. The dependence of the zeta potentials of MnO$_2$ and RGO upon pH is present in Figure 6-9. The zeta potential of MnO$_2$ first deceases (pH = 1.8 to 7.5), and then increases (pH = 7.5 to 11.8). The stability of MnO$_2$ colloid decreases at pH from 7.5 to 11.8. RGO colloid has the opposite behavior in this region (pH from 7.5 to 11.8), and its stability increases with pH. Therefore, the MnO$_2$/RGO mixture was kept at pH 11 and without severely stirring.

The lamellar structures of RGO and MnO$_2$ were evident from their AFM and TEM images (Figure 6-8). The height profile scans of AFM images of MnO$_2$

and RGO (Figure 6-8b and c) present a fairly flat surface of both samples with approximate thicknesses of 4.5 nm and 1.3 nm, respectively. The lateral size of RGO is much larger than MnO_2 (Figure 6-8d and e). The RGO sheets with large area and flat morphology serve as ideal microscopic substrates to host the MnO_2. The synergic effects of the electrostatic interaction and flat morphology between the MnO_2 nanosheets and RGO realized the integration of MnO_2 nanosheets onto graphene surfaces.[42] Indeed, Figure 6-8f displays that the MnO_2 nanosheets attach to the surface of RGO, instead of aggregating themselves.
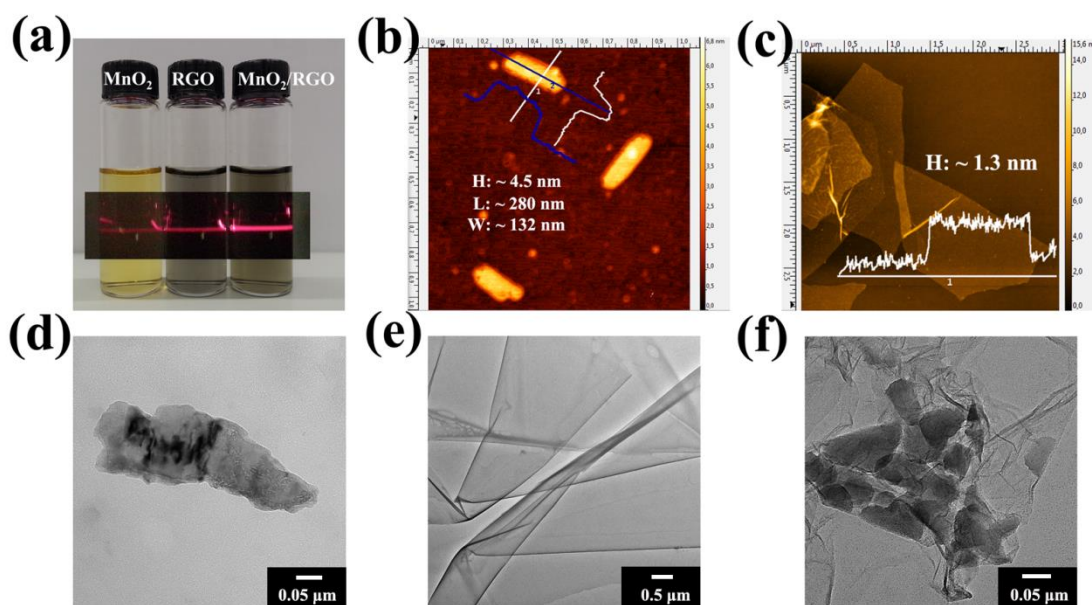

Figure 6-8 (a) Photograph of the aqueous colloidal suspensions of MnO₂, RGO and MnO₂/RGO, showing Tyndall effect when the red lacer goes through, AFM images of (b) MnO₂ and (c) RGO, TEM images of (e) MnO₂, (f) RGO and (g) MnO₂/RGO.
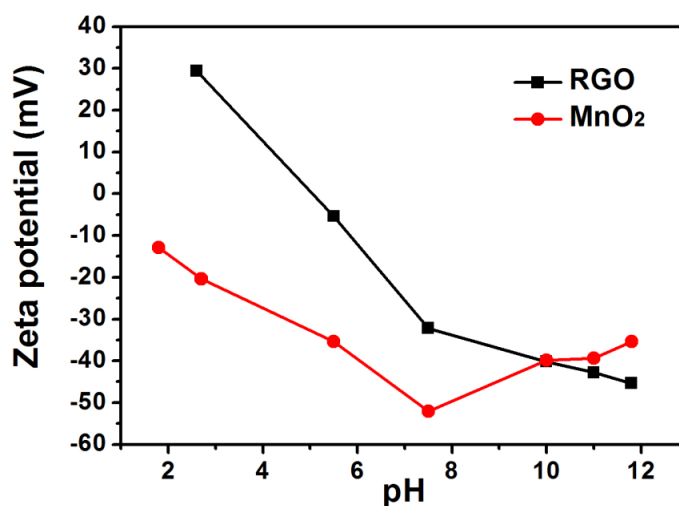

Figure 6-9 Zeta potential of RGO and MnO₂ as a function of pH, in aqueous dispersion, adjusted by HCl and NH₃·H₂O
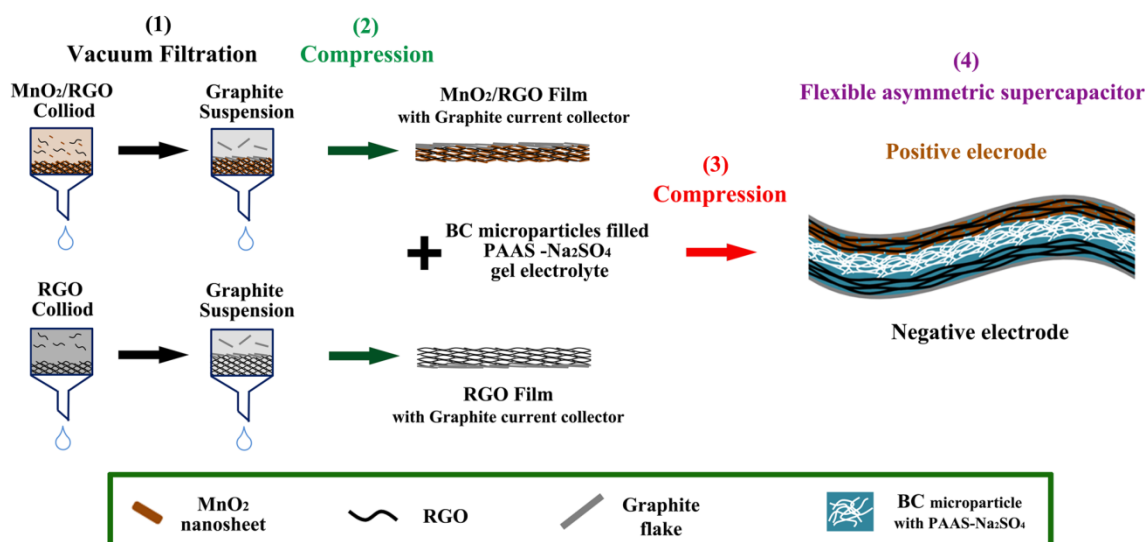
Figure 6-10 Schematic illustration of the preparation process. (1) Vacuum filtration of MnO$_2$/RGO, RGO colloidal suspensions and graphite flakes suspension, (2) Compression to obtain MnO$_2$/RGO and RGO hydrogel films with attached graphite current collector, (3) Compression to assemble the flexible SC with obtained hydrogel films and BC/PAAS-Na$_2$SO$_4$ gel electrolyte, (4) Schematic structure of the assembled flexible asymmetric SC, demonstrating the role of separation of BC clusters.

Figure 6-10 demonstrates the fabrication of the flexible asymmetric SC. MnO$_2$/RGO (positive electrode) and RGO (negative electrode) hydrogel films are prepared by vacuum filtration of MnO$_2$/RGO and RGO colloidal suspensions, respectively. The graphite current collector is deposited by the successive filtration of graphite flakes suspension. Figure 6-11a and b show SEM images of the cross-section of MnO$_2$/RGO and RGO films with the graphite current collector on the top surface. They both have a layer-by-layer structure, which benefits from the pilling of 2D MnO$_2$ and RGO, or just RGO. The cross-section SEM images of the assembled SC (Figure 6-11c and 6-11d) show the sandwich-like structure. In order to achieve a high flexibility for the final device, the thicknesses of both electrodes are limited to a few tens of micrometers as well as the gel electrolyte after the compression (Figure 6-11d).

BC/PAAS-Na$_2$SO$_4$ gel electrolyte plays a significant role in flexible SCs, where two electrodes have to be sticked with each other by the gel electrolyte, but prevented from the short circuit (Figure 6-10). The BC clusters soaked by PAA gel (Figure 6-11e) take the responsibility for separating two electrodes. The image of BC/PAAS-Na$_2$SO$_4$ gel electrolyte and its rheology behavior are demonstrated in Figure 6-11f. It shows a very high viscosity (~ 10^4 Pa s) and low dependence on the temperature. High viscosity and sticky property of gel electrolyte can combine two electrodes together, preventing them from the split-up under the cycling of bending.
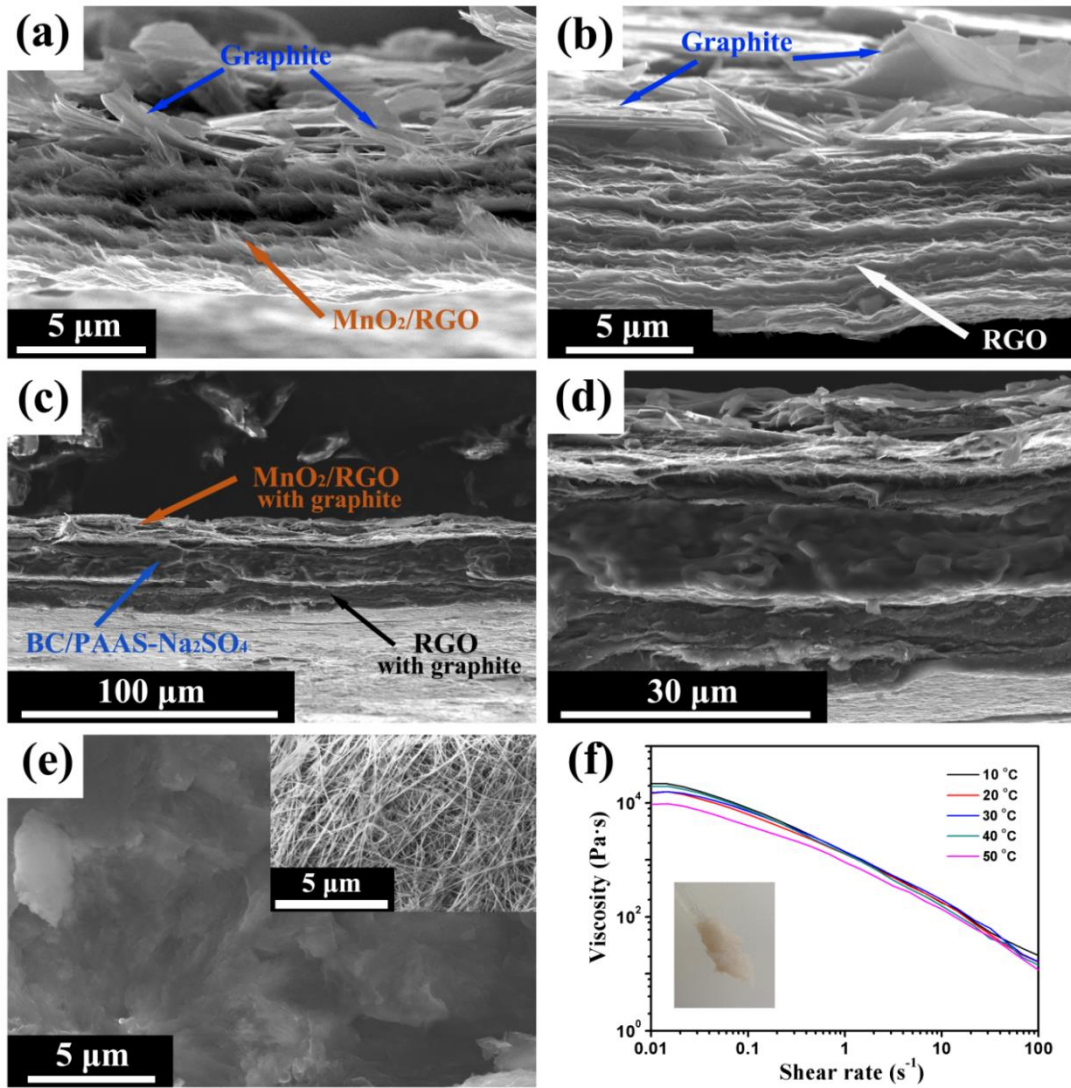
Figure 6-11 SEM images of the cross-section of MnO₂/RGO (a) and RGO (b) hydrogel films with graphite current collectors, and (c) the assembled SC and (d) at high magnification, and (e) the BC/PAAS-Na₂SO₄ gel electrolyte (inset image shows the BC nanofibers in BC cluster), (f) effect of the viscosity of BC/PAAS-Na₂SO₄ gel electrolyte on shear rate at varcvious temperatures (Inset shows the digital image of this gel electrolyte).

First of all, cyclic voltammetry was used to estimate the potential window of each electrode (MnO₂/RGO and RGO) in a three-electrode system (Figure 6-12a). The stable potential window is between -1.0 and 0 V for RGO and between 0 and 0.8 V for MnO₂/RGO, which indicates the fabricated cell can achieve an extended potential range of 1.8 V. To obtain such operating voltage, to keep the amount of charges, Q, stored in the positive and negative electrodes the same is necessary. It can be expressed by the following equation:

$$Q = C_{sp}{}^+ \times m^+ \times \Delta U^+ = C_{sp}{}^- \times m^- \times \Delta U^-$$

where ΔU^+ and ΔU^-, represent the potential window of positive and negative electrodes, respectively, during the operation of the SC. Thus the mass ratio of

two electrodes can be calculated by the equation:

$$m^-/m^+ = C_{sp}{}^+ \times \Delta U^+ = C_{sp}{}^- \times \Delta U^-$$

since the $C_{sp}{}^+$ of MnO$_2$/RGO is 164 F g^{-1} and the $C_{sp}{}^-$ of RGO is 87 F g^{-1} calculated from the CV profiles in Figure 6-12a, the weight ratio (m^-/m^+) of RGO and MnO$_2$/RGO was kept to 1.5 in the asymmetric SC cell according to the above equation.
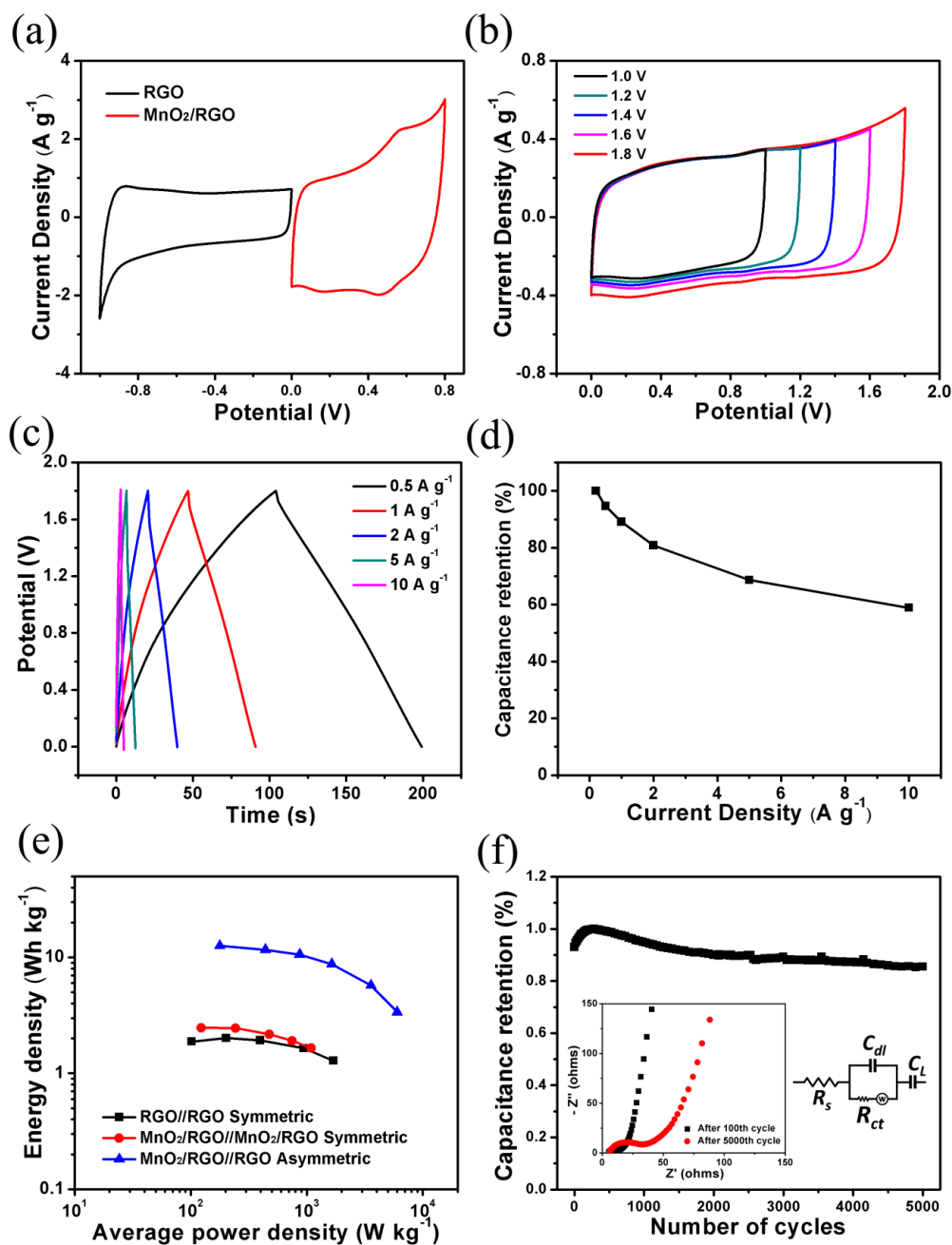

Figure 6-12 (a) CV curves of RGO and MnO$_2$/RGO at a scan rate of 10 mV s^{-1} collected in a three-electrode system with an Ag/AgCl reference in 1 M Na$_2$SO$_4$. Electrochemical performance of the assembled flexible asymmetric SC of MnO$_2$/RGO//RGO: (b) CV curves at a scan rate of 10 mV s^{-1} with different potential

window, (c) Galvanostatic charge-discharge curves at various current densities from 0.5 A g^{-1} to 10 A g^{-1}, (d) Capacitance retention as a function of discharge currents. (e) Ragone plots of the asymmetric cell of MnO$_2$/RGO//RGO (1.8 V), the symmetric ones of RGO//RGO (1 V) and MnO$_2$/RGO// MnO$_2$/RGO (0.8 V). (f) Cycling stability of MnO$_2$/RGO//RGO at a current density of 1 A g^{-1} (Inset image shows Nyquist plots before and after 5000 cycles, and the electrical equivalent circuit used for fitting impedance spectra).

As expected, the fabricated asymmetric SC can achieve a wide voltage up to 1.8 V shown in Figure 6-12b. Galvanostatic charge/discharge curves at different current densities in a potential window of 0 - 1.8 V (Figure 6-12c) indicate that this asymmetric SC has an excellent capacitive behavior with rapid I-V response. The specific capacitance (*Ct*) of the asymmetric SC is calculated to be 27 F g^{-1} (*C$_A$*, 29 mF cm^{-2}) based on the total mass of active materials in the two electrodes at a current density of 0.5 A g^{-1} and still reaches 17 F g^{-1} (18 mF cm^{-2}) at a high current density of 10 A g^{-1}. Ragone plots, depicting the relation between power density (P) and energy densities (E), were used to evaluate the performance of the three types of SCs, RGO//RGO, MnO$_2$/RGO//MnO$_2$/RGO symmetric, and MnO$_2$/RGO//RGO asymmetric SCs (Figure 6-12e). The energy density of MnO$_2$/RGO//RGO asymmetric SCs (1.8 V) is much higher than those of RGO//RGO, MnO$_2$/RGO//MnO$_2$/RGO symmetric SCs (1 V and 0.8 V, respectively). For instance, at a current density of 0.5 A g^{-1}, the energy density of MnO$_2$/RGO//RGO (11.7 Wh kg^{-1}) is about 4-fold increase, compared to that of RGO//RGO (1.9 Wh kg^{-1}) and MnO$_2$/RGO//MnO$_2$/RGO (2.1 Wh kg^{-1}). The energy density of MnO$_2$/RGO//RGO is comparable to those asymmetric SCs based on general MnO$_2$ composite electrode[22, 60], however, smaller than those based on electrochemically prepared MnO$_2$.[25, 59] The disadvantages of the electrochemical technique are their limit to the large-scale preparation and their obtained nanostructured MnO$_2$ layers are brittle on the flexible substrate upon the increase of deposition.[61] Instead, this assembled SC has an excellent flexibility, which will be discussed afterward. In addition, MnO$_2$/RGO//RGO exhibits excellent cycling stability. This cell shows good capacitance retention of 85.5 % over the highest capacitance after 5000 cycles. A capacitance increase can be observed in the first 100 cycles, which is ascribed to the cation intercalation/deintercalation in two-dimensional layered MnO$_2$.[62, 63] This behavior endows the CV curve of MnO$_2$/RGO having a redox pair at about 0.5 V and 0.6 V (Figure 6-12a) and exhibiting higher capacitance.

Because of the optimized structural design, mainly the reduction of the thickness of the final device (about 120 μm including the PE substrates) by

thinning both of the electrodes and gel electrolyte, this asymmetric SC exhibits a high flexibility and an excellent cycling stability on the deformation. Figure 6-13a show its CV curves in different deformation states. CV curves exhibit a similar rectangle shape and only a slight shifting can be observed. In addition, the capacitance retentions of the device after bending and rolling for various times are presented in Figure 6-13c. There is no significant decrease of specific capacitance occurring, which indicates no huge damage has taken place during the cycling test. Figure 6-13d shows a packing cell with two $MnO_2/RGO//RGO$ asymmetric SCs in series (3.6 V), which is able to light a light-emitting diode (LED) lamp with a forward voltage of 2.7 V. The rolling of the flexible SC has no obvious effect on the performance of the LED.
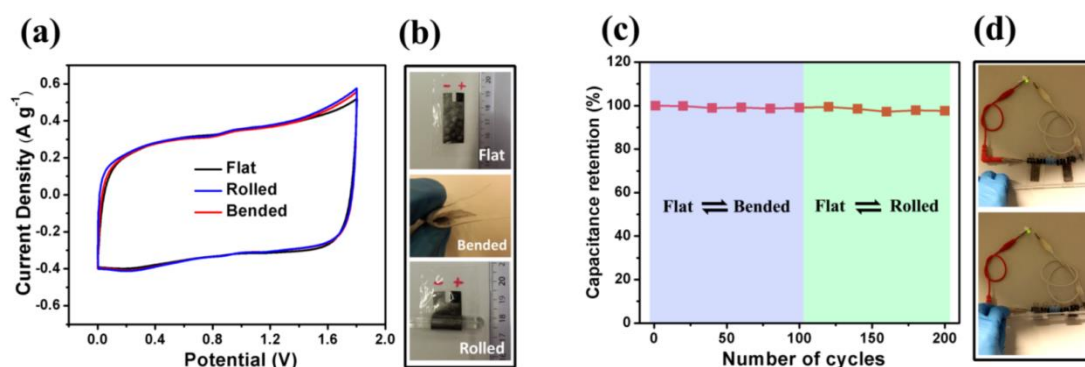

Figure 6-13 Flexibility of asymmetric $MnO_2/RGO//RGO$ device. (a) CV curves at 10 mV s^{-1} at three different bending state: (b) flat, bended and rolled. (c) Capacitance retention after cycles of repeating flat/bended and flat/rolled. (d) Photograph displays a green light-emitting diode (LED) lighted by two asymmetric cells in series and demonstrates no obvious performance change of LED from the flat state to rolled state.

Conclusion

A highly flexible asymmetric SC has been fabricated using 2D MnO_2 and RGO piled hydrogel films and a $BC/PAAS-Na_2SO_4$ neutral gel electrolyte. This SC device demonstrates a high flexibility, where bending and even rolling have no obvious effect on its electrochemical performance. Here, $BC/PAAS-Na_2SO_4$ gel electrolyte plays a significant role in the combination and separation of two electrodes to achieve such flexibility. By asymmetric configuration, the cell voltage of this flexible SC has been extended to 1.8 V, and the energy density can reach up to 11.7 Wh kg^{-1}, which enhances its potential for practical application. This SC is economical and environmentally friendly due to the use of low-cost MnO_2 and no harmful neural gel electrolyte. However, in order to obtain high flexibility, the low mass loading of active materials is required, which results in a low areal capacitance (29 mF cm^{-2}). Therefore, finding compromise between flexibility and the electrochemical performance of a flexible SC is a goal for the future work.

6.3 In-situ preparation of bacterial cellulose reinforced hydrogel electrolyte for flexible supercapacitors

In this study, one bacterial cellulose (BC) reinforced hydrogel electrolyte with a double network structure created by PAA and SA is reported. The PAA network was covalently crosslinked by poly(ethylene glycol) diacrylate (PEGDA), while the SA network was ionically crosslinked by Ca^{2+}. Moreover, BC clusters, a biopolymer with an inherent network structure, was also added to reinforce further its mechanical property. Finally, a flexible SC was achieved directly by in-situ preparation of this hydrogel electrolyte on two RGO hydrogel based flexible electrodes. The resultant hydrogel electrolyte demonstrates an improved mechanical property and promising performance in flexible SCs.
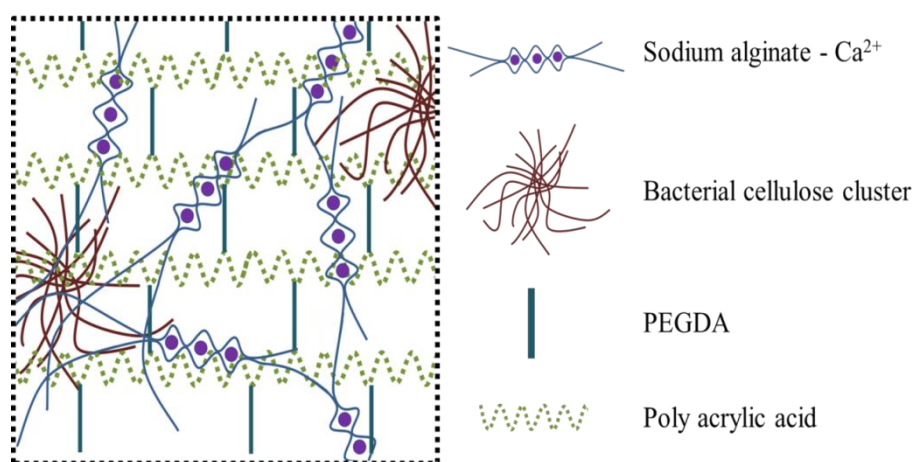

Figure 6-14 Schematic diagram e of the internal structure of PAA/SA-Ca/BC hydrogel, showing the double-network of PAA and Ca^{2+} cross-linked SA and the entanglement by BC clusters.

The schematic diagram in Figure 6-14 demonstrates the methology of the preparation of this BC reinforced hydrogel electrolyte. It has a double-network. The first network is created by chemically crosslinked PAA. The crosslink agent is PEGDA (average M_n 250), which has a much longer polymer chain than common crosslinker, N,N′-Methylenebis (acrylamide). It tends to soften the obtained PAA network, which is served as the 'soft' part in this double-network. The second network is constructed by SA, served as the 'hard' part. In order to get a well-connected SA network, two steps of crosslinking were applied. The first step of crosslinking was achieved by $CaSO_4$. After the capture of SA gel into the PAA hdyrgel, a low but uniform crosslinked SA network generates due to the slow release of Ca^{2+} ions of $CaSO_4$. The second step of crosslinking of SA was completed by massive Ca^{2+} with fast mobilty in $CaCl_2$ solution, which can dramaticly increase the degree of crosslinking. The pre-crosssslink by $CaSO_4$ ensures the process of second crosslinking, preventing from the shrinking and nonuniform crosslinking. Moreover, the BC clusters were added to

entanglement the chains of these double-network to further enhance the mechanical property.

The ATR-FTIR spectrum of PAA/SA-Ca/BC is shown in Figure 6-15. For the comparison, the spectra of pure PAA, SA and BC are also included. For SA, the peak for carboxylate group appears at 1605 cm^{-1}. These corresponding peaks are obviously found in the spectrum of PAA/SA-Ca/BC. However, the peak for carboxylate group is altered slightly to 1557 cm^{-1} due to the ionic crosslinking with Ca^{2+}.[65]
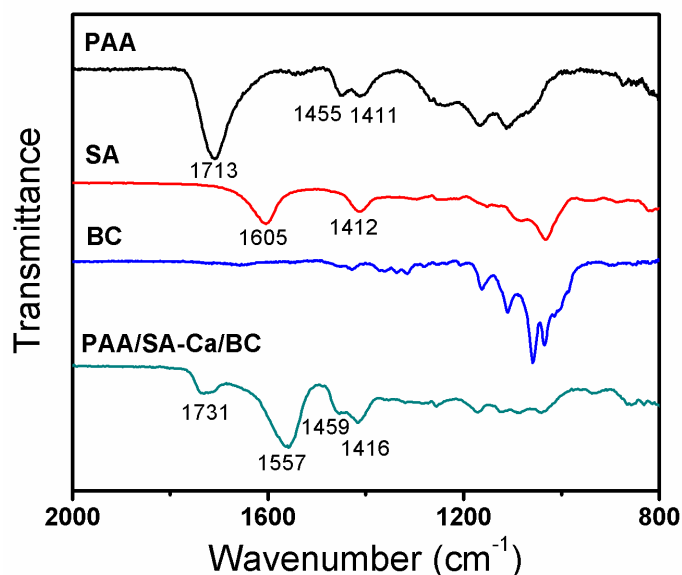

Figure 6-15 ATR-FTIR spectra of pure PAA, SA, BC and PAA/SA-Ca/BC
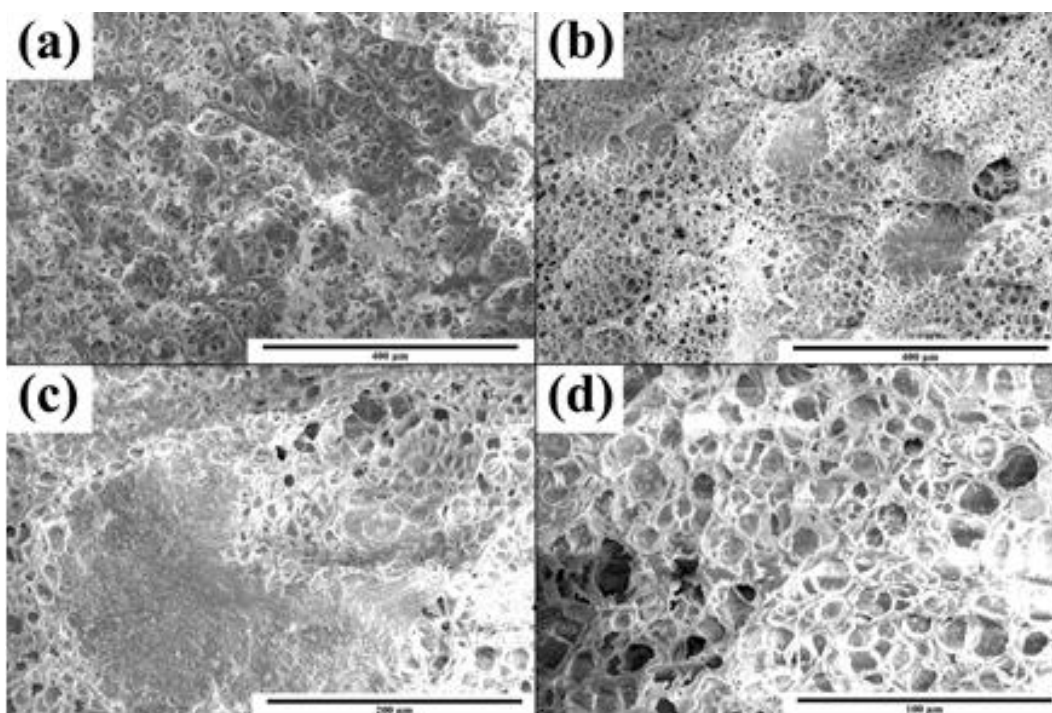

Figure 6-16 SEM images of (a) PAA/SA-Ca and (b) (c) (d) PAA/SA-Ca/BC

The morphology of PAA/SA-Ca and PAA/SA-Ca/BC is shown in Figure 6-16. It can be seen in Figure 6-15(a) and (b) that both the hydrogels exhibit high porous structure. In case of PAA/SA-Ca/BC shown in Figure 6-15(b), BC clusters present in the network, acting as knots, which indicates that BC improve the mechanical property. PAA/SA-Ca/BC exhibits more uniform porous structure shown in Figure 6-15(d). A uniform and highly porous structure endows hydrogel electrolytes (PAA/SA-Ca/BC) having a high ionic conductivity as well.
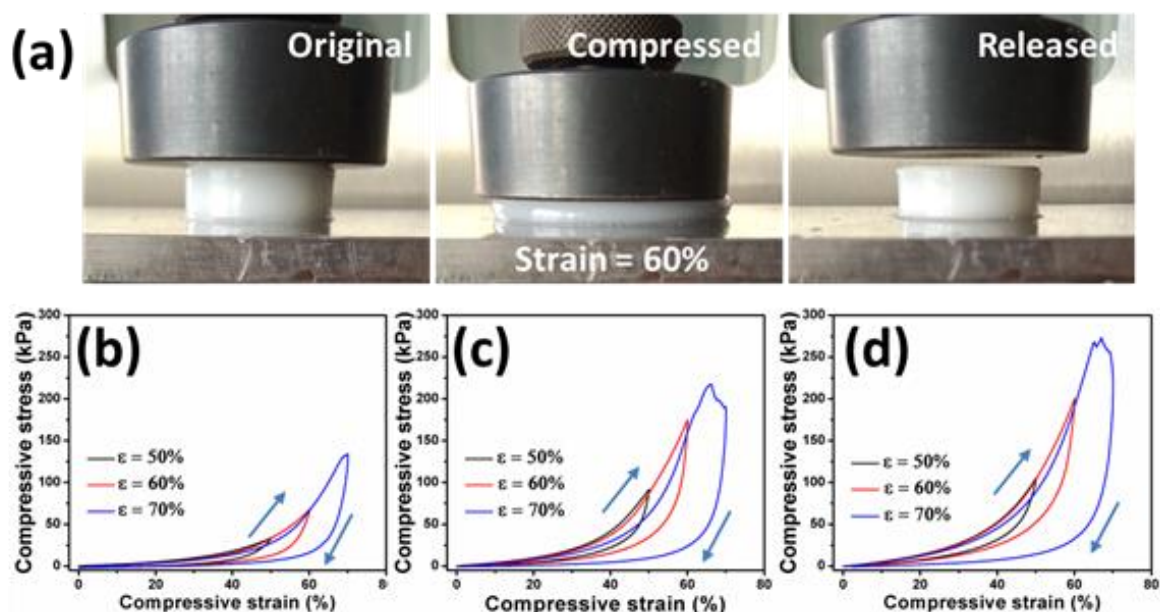

Figure 6-17 Compressive mechanical properties of prepared hydrogel electrolytes. (a) Images of compressive process of PAA/SA-Ca/BC hydrogel. Compressive stress as a function of strain from cycling compressive test of (b) PAA/SA-CaSO₄, (c) PAA/SA-Ca and (d) PAA/SA-Ca/BC

Figure 6-17(a) shows the process of compressive test using an example of PAA/SA-Ca/BC hydrogel. The hydrogel was compressed to the required strain and then released to the initial state. Several cycles (strain = 50 %, 60 % and 70 %) have been conducted until the hydrogel being fractured. PAA/SA-Ca/BC hydrogel exhibits excellent compressive property with a strain of 60 % (Figure 6-17(a)). Three samples exhibit similar compressive behaviors (Figure 6-17(b), (c) and (d)). They have good reversibility within strains of 50 % and 60 % and break down when the strain goes up to 70 %. However, the maximum compressive stress of each cycle is different. With the assistance of further ionic crosslink of $CaCl_2$, PAA/SA-Ca achieved a compressive stress up to 217 kPa compared to PAA/SA-CaSO₄ of 134 kPa. Moreover, with the reinforcement of BC clusters, PAA/SA-Ca/BC exhibits a compressive stress of 273 kPa.

After the in-situ preparation, PAA/SA-Ca/BC hydrogel electrolyte wraps two RGO/G flexible electrodes, combining them together. This SC demonstrates some flexibility. However, due to the high thickness (around a centimeter), the

flexibility is limited. What is worse, there is low adhesion between the hydrogel electrolyte and flexible electrodes. During the bending, it tends to be several individual layers. In the further study, the reduction of the thickness of hydrogel electrolyte and the enhancement of the connection of hydrogel through the electrode layer are suggested.

Ionic conductivity of PAA/SA-Ca/BC was measured by electrochemical impedance spectroscopy (EIS) and calculated using the following equation: $\sigma_0 = L/RA$, where L, R and A are the thickness, bulk resistance and area of the hydrogel electrolyte, respectively. The ionic conductivity of PAA/SA-Ca/BC is 0.035 S cm^{-1} compared to that of 2 M KCl (0.04 S cm^{-1}). Figure 6-18(a) shows the CV curves of assembled SCs with electrolyte of 1 M KCl, 2 M KCl and PAA/SA-Ca/BC, respectively. Rare difference is observed between these three electrolytes. Figure 6-18(b) displays their Nyquist plots. It indicates that the prepared PAA/SA-Ca/BC hydrogel electrolyte has a very similar electrochemical performance to their liquid electrolytes.
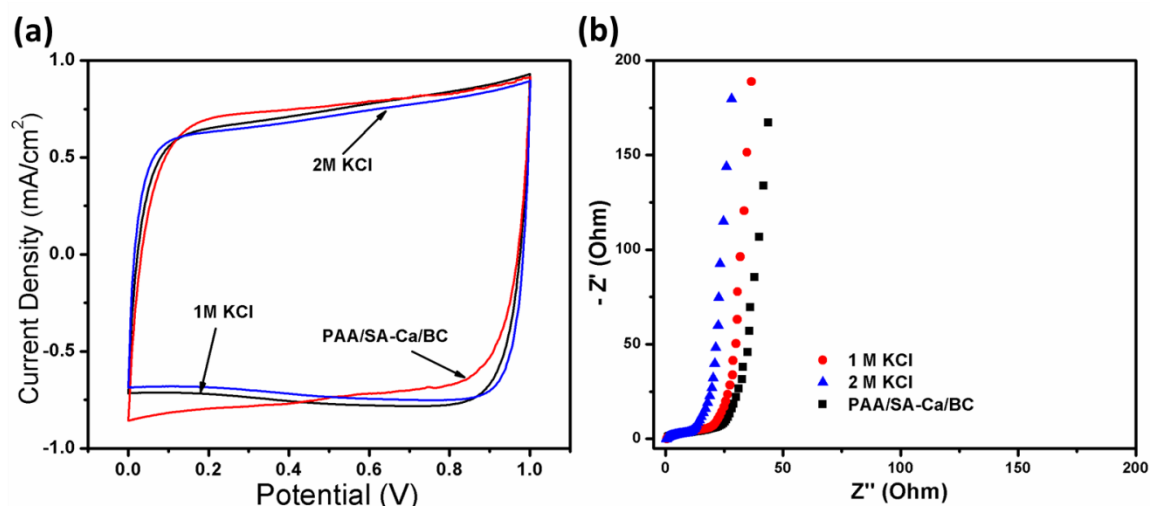

Figure 6-18 (a) CV curves and (b) Nyquist plots of SCs with electrolyte of 1M KCl, 2M KCl and PAA/SA-Ca/BC, respectively

Conclusion

PAA/SA-Ca/BC hydrogel electrolyte has been prepared with an improved mechanical property. Its mechanical property highly improved not only due to ionic crosslink of SA but also the reinforcement of BC clusters. The compressive stress can reach up to 273 kPa. This hydrogel electrolyte exhibits a low shrinkage of 93 % in 2 M KCl. Moreover, it has a high ionic conductivity of 0.035 S cm^{-1}. Subsequently, PAA/SA-Ca/BC was in-situ prepared into a flexible SC device, which displays similar electrochemical performances to liquid electrolyte. It indicates that PAA/SA-Ca/BC hydrogel electrolyte has a positive possibility to replace KCl liquid electrolyte. However, the flexibility of the prepared flexible SCs is limited, due to the structural design and the bad interaction between the electrodes and hydrogel electrolyte.

6.4 Summary and outlook

Throughout the text, several conclusions and suggestions are given in this section, helpful to the further study of flexible SCs.

First, porous structure of RGO hydrogel is described as it enhances the ions' diffusion without decreasing SSA, which generally occurs in the three-dimensional RGO foams caused by partial restacking during the freeze-drying. It is a simple approach to obtain porous structural RGO without assisted templates. The obtained RGO hydrogel could be an ideal conductive matrix for other pseudo-capacitive materials to deposit on the surface. To this end, the diffusion of monomers has to be considered to make sure a uniform coating of pseudo-capacitive materials from the surface to the internal of RGO hydrogel. This kind of prepared RGO composite hydrogel seems to be excellent electrode for SCs. However, for its low mechanical property, despite that several strategies were implemented in this study as well as others; more efforts have to be done in the future for its practical application in flexible electrodes.

The importance of current collectors should be highlighted. For these free-standing electrodes which have high thickness, the use of metal foils or substrates with deposited current collectors seems not to an optimum choice due to the mechanical analysis. The direct deposition of ultrathin current collectors on free-standing electrodes is considered as a promising approach. For RGO hydrogel, because of the water absorbed, it is difficult for them to connect to the circuit. In this study, graphite current collector can directly deposit on its surface by intercalated into the stand-up RGO nanosheets. It is also promising to be the transition layer between RGO and metal current collector for a better contact to enhance the power of prepared SC devices.

Flexible electrodes' thickness can be reduced by using 2D nanomaterials because of the layer-by-layer pilling. In the case of RGO hydrogel, the reduction of the thickness may not be that significant due to the separation of water molecular. And a certain degree of restacking is necessary to improve the mechanical property. Thus, it is suggested to use restacked 2D nanomaterials with high specific capacitance and well controlled deposited thickness. In order to solve the weak ion diffusion, the planar configuration and etching methods for preparing of micro interdigitated electrodes are recommended.

In the sandwich-type configuration, the separation and the combination of two flexible electrodes are both important for the gel/hydrogel electrolyte to achieve. For gel electrolytes, the challenge is the separation, while for hydrogel electrolyte is the combination. For both of them, the reduction of their thickness is essential. In this study, the obtained PAAS-Na$_2$SO$_4$/BC gel electrolyte has played a good role in both aspects. It works well on the function of separation in RGO hydrogel based electrodes, which has a flat surface. It is worthy to study its performance in the flexible electrodes with rough surface.

Finally, by using thinner and softer flexible substrate increases the flexibility of the obtained electrodes. However, the reduction of other properties such as elongation, anti-puncture and abrasion resistance could take a risk in the protection of the electrodes. In addition, the location of the flexible SCs in the integrated circuit board or other device should be considered, because it changes the mechanical neutral plane which is significant to prevent from the fragmentation of electrodes.

REFERENCES

[1] Nathan A., Ahnood A., Cole M. T., Lee S., Suzuki Y., Hiralal P., Bonaccorso F., Hasan T., Garcia-Gancedo L., Dyadyusha A., Haque S., Andrew P., Hofmann S., Moultrie J., Chu D., Flewitt A. J., Ferrari A. C., Kelly M. J., Robertson J., Amaratunga G. A. J. and Milne W. I., *Flexible Electronics: The Next Ubiquitous Platform*. Proceedings of the IEEE, [online]. 2012, vol. 100, issue Special Centennial Issue, pp. 1486-1517. Availble from: 10.1109/JPROC.2012.2190168.

[2] Bae S., Kim H., Lee Y., Xu X., Park J.-S., Zheng Y., Balakrishnan J., Lei T., Ri Kim H., Song Y. I., Kim Y.-J., Kim K. S., Ozyilmaz B., Ahn J.-H., Hong B. H. and Iijima S., *Roll-to-roll production of 30-inch graphene films for transparent electrodes*. Nat Nano, [online]. 2010, vol. 5, issue 8, pp. 574-578. Availble from: doi:10.1038/nnano.2010.132.

[3] Lee Y., Min S.-Y., Kim T.-S., Jeong S.-H., Won J. Y., Kim H., Xu W., Jeong J. K. and Lee T.-W., *Versatile Metal Nanowiring Platform for Large-Scale Nano- and Opto-Electronic Devices*. Advanced Materials, [online]. 2016, vol. 28, issue 41, pp. 9109-9116. Availble from: 10.1002/adma.201602855.

[4] Aleksandrova M., *Specifics and Challenges to Flexible Organic Light-Emitting Devices*. Advances in Materials Science and Engineering, [online]. 2016, vol. 2016, issue pp. 8. Availble from: 10.1155/2016/4081697.

[5] Hammock M. L., Chortos A., Tee B. C. K., Tok J. B. H. and Bao Z., *25th Anniversary Article: The Evolution of Electronic Skin (E-Skin): A Brief History, Design Considerations, and Recent Progress*. Advanced Materials, [online]. 2013, vol. 25, issue 42, pp. 5997-6038. Availble from: 10.1002/adma.201302240.

[6] Amar A., Kouki A. and Cao H., *Power Approaches for Implantable Medical Devices*. Sensors, [online]. 2015, vol. 15, issue 11, pp. 28889. Availble from: 10.3390/s151128889.

[7] Nyholm L., Nystrom G., Mihranyan A. and Stromme M., *Toward flexible polymer and paper-based energy storage devices*. Adv Mater, [online]. 2011, vol. 23, issue 33, pp. 3751-69. Availble from: 10.1002/adma.201004134.

[8] Zhou G., Li F. and Cheng H.-M., *Progress in flexible lithium batteries and future prospects*. Energy Environ. Sci., [online]. 2014, vol. 7, issue 4, pp. 1307-1338. Availble from: 10.1039/c3ee43182g.

[9] Shao Y., El-Kady M. F., Wang L. J., Zhang Q., Li Y., Wang H., Mousavi M. F. and Kaner R. B., *Graphene-based materials for flexible supercapacitors*. Chem. Soc. Rev., [online]. 2015, vol. 44, issue 11, pp. 3639-65. Availble from: 10.1039/c4cs00316k.

[10] Zhang L. L. and Zhao X. S., *Carbon-based materials as supercapacitor electrodes*. Chemical Society Reviews, [online]. 2009, vol. 38, issue 9, pp. 2520-2531. Availble from: 10.1039/B813846J.

[11] Afzal A., Abuilaiwi F. A., Habib A., Awais M., Waje S. B. and Atieh M. A., *Polypyrrole/carbon nanotube supercapacitors: Technological advances and challenges*. Journal of Power Sources, [online]. 2017, vol. 352, issue pp. 174-186. Availble from: http://doi.org/10.1016/j.jpowsour.2017.03.128.

[12] Wen L., Li F. and Cheng H.-M., *Carbon Nanotubes and Graphene for Flexible Electrochemical Energy Storage: from Materials to Devices*. Adv. Mater., [online]. 2016, vol. 28, issue 22, pp. 4306-4337. Availble from: 10.1002/adma.201504225.

[13] Wang H., Zhang Y., Sun W., Tan H. T., Franklin J. B., Guo Y., Fan H., Ulaganathan M., Wu X.-L., Luo Z.-Z., Madhavi S. and Yan Q., *Conversion of uniform graphene oxide/polypyrrole composites into functionalized 3D carbon nanosheet frameworks with superior supercapacitive and sodium-ion storage properties*. Journal of Power Sources, [online]. 2016, vol. 307, issue pp. 17-24. Availble from: http://dx.doi.org/10.1016/j.jpowsour.2015.12.104.

[14] Moussa M., El-Kady M. F., Zhao Z., Majewski P. and Ma J., *Recent progress and performance evaluation for polyaniline/graphene nanocomposites as supercapacitor electrodes*. Nanotechnology, [online]. 2016, vol. 27, issue 44, pp. 442001. Availble from: 10.1088/0957-4484/27/44/442001.

[15] Simon P. and Gogotsi Y., *Materials for electrochemical capacitors*. Nat. Mater., [online]. 2008, vol. 7, issue 11, pp. 845-854. Availble from:

[16] Chang S.-J., Hyun M. S., Myung S., Kang M.-A., Yoo J. H., Lee K. G., Choi B. G., Cho Y., Lee G. and Park T. J., *Graphene growth from reduced graphene oxide by chemical vapour deposition: seeded growth accompanied by restoration*. Scientific Reports, [online]. 2016, vol. 6, issue pp. 22653. Availble from: 10.1038/srep22653.

[17] Xiong C., Li T., Zhao T., Dang A., Li H., Ji X., Jin W., Jiao S., Shang Y. and Zhang Y., *Reduced graphene oxide-carbon nanotube grown on carbon fiber as binder-free electrode for flexible high-performance fiber supercapacitors*. Composites Part B: Engineering, [online]. 2017, vol. 116, issue pp. 7-15. Availble from: http://dx.doi.org/10.1016/j.compositesb.2017.02.028.

[18] Wang G., Sun X., Lu F., Sun H., Yu M., Jiang W., Liu C. and Lian J., *Flexible Pillared Graphene-Paper Electrodes for High-Performance*

Electrochemical Supercapacitors. Small, [online]. 2012, vol. 8, issue 3, pp. 452-459. Availble from: 10.1002/smll.201101719.

[19] Xu Y., Lin Z., Huang X., Liu Y., Huang Y. and Duan X., *Flexible Solid-State Supercapacitors Based on Three-Dimensional Graphene Hydrogel Films*. ACS Nano, [online]. 2013, vol. 7, issue 5, pp. 4042-4049. Availble from: 10.1021/nn4000836.

[20] Peng X., Peng L., Wu C. and Xie Y., *Two dimensional nanomaterials for flexible supercapacitors*. Chem. Soc. Rev., [online]. 2014, vol. 43, issue 10, pp. 3303-3323. Availble from: 10.1039/C3CS60407A.

[21] Pandolfo T., Ruiz V., Sivakkumar S. and Nerkar J., *General Properties of Electrochemical Capacitors,* Wiley-VCH Verlag GmbH & Co. KGaA, 2013, 9783527646661

[22] Brousse T., Taberna P.-L., Crosnier O., Dugas R., Guillemet P., Scudeller Y., Zhou Y., Favier F., Bélanger D. and Simon P., *Long-term cycling behavior of asymmetric activated carbon/MnO2 aqueous electrochemical supercapacitor*. J. Power Sources, [online]. 2007, vol. 173, issue 1, pp. 633-641. Availble from: 10.1016/j.jpowsour.2007.04.074.

[23] Simon P., Gogotsi Y. and Dunn B., *Where Do Batteries End and Supercapacitors Begin?* Science, [online]. 2014, vol. 343, issue 6176, pp. 1210-1211. Availble from: 10.1126/science.1249625.

[24] Wang G., Zhang L. and Zhang J., *A review of electrode materials for electrochemical supercapacitors*. Chem. Soc. Rev., [online]. 2012, vol. 41, issue 2, pp. 797-828. Availble from: 10.1039/c1cs15060j.

[25] El-Kady M. F., Ihns M., Li M., Hwang J. Y., Mousavi M. F., Chaney L., Lech A. T. and Kaner R. B., *Engineering three-dimensional hybrid supercapacitors and microsupercapacitors for high-performance integrated energy storage*. Proc. Natl. Acad. Sci. U. S. A., [online]. 2015, vol. 112, issue 14, pp. 4233-8. Availble from: 10.1073/pnas.1420398112.

[26] Byun S. and Yu J., *Direct formation of a current collector layer on a partially reduced graphite oxide film using sputter-assisted metal deposition to fabricate high-power micro-supercapacitor electrodes*. Journal of Power Sources, [online]. 2016, vol. 307, issue pp. 849-855. Availble from: 10.1016/j.jpowsour.2016.01.054.

[27] Yan J., Wang Q., Wei T. and Fan Z., *Recent Advances in Design and Fabrication of Electrochemical Supercapacitors with High Energy Densities*. Advanced Energy Materials, [online]. 2014, vol. 4, issue 4, pp. 1300816-n/a. Availble from: 10.1002/aenm.201300816.

[28] Long J. W., Bélanger D., Brousse T., Sugimoto W., Sassin M. B. and Crosnier O., *Asymmetric electrochemical capacitors—Stretching the limits of aqueous electrolytes*. MRS Bull., [online]. 2011, vol. 36, issue 07, pp. 513-522. Availble from: 10.1557/mrs.2011.137.

[29] Piñeiro-Prado I., Salinas-Torres D., Ruiz-Rosas R., Morallón E. and Cazorla-Amorós D., *Design of Activated Carbon/Activated Carbon Asymmetric*

Capacitors. Frontiers in Materials, [online]. 2016, vol. 3, issue 16, pp. Availble from: 10.3389/fmats.2016.00016.

[30] Taberna P.-L. and Simon P., *Electrochemical Techniques,* Wiley-VCH Verlag GmbH & Co. KGaA, 2013, 9783527646661

[31] Gleskova H., Cheng I. C., Wagner S. and Suo Z., *Mechanical Theory of the Film-on-Substrate-Foil Structure: Curvature and Overlay Alignment in Amorphous Silicon Thin-Film Devices Fabricated on Free-Standing Foil Substrates,* Springer Science & Business Media, 2009, 978-0-387-74362-2

[32] Suo Z., Ma E. Y., Gleskova H. and Wagner S., *Mechanics of rollable and foldable film-on-foil electronics*. Appl. Phys. Lett., [online]. 1999, vol. 74, issue 8, pp. 1177-1179. Availble from: 10.1063/1.123478.

[33] Mao L., Meng Q., Ahmad A. and Wei Z., *Mechanical Analyses and Structural Design Requirements for Flexible Energy Storage Devices*. Advanced Energy Materials, [online]. vol. issue pp. n/a-n/a. Availble from: 10.1002/aenm.201700535.

[34] Zhang H., Qiao Y. and Lu Z., *Fully Printed Ultraflexible Supercapacitor Supported by a Single-Textile Substrate*. ACS Appl. Mater. Interfaces, [online]. 2016, vol. 8, issue 47, pp. 32317-32323. Availble from: 10.1021/acsami.6b11172.

[35] Xu C., Xu B., Gu Y., Xiong Z., Sun J. and Zhao X. S., *Graphene-based electrodes for electrochemical energy storage*. Energy & Environmental Science, [online]. 2013, vol. 6, issue 5, pp. 1388-1414. Availble from: 10.1039/C3EE23870A.

[36] Li D., Muller M. B., Gilje S., Kaner R. B. and Wallace G. G., *Processable aqueous dispersions of graphene nanosheets*. Nat. Nanotechnol., [online]. 2008, vol. 3, issue 2, pp. 101-5. Availble from: 10.1038/nnano.2007.451.

[37] Maiti U. N., Lim J., Lee K. E., Lee W. J. and Kim S. O., *Three-dimensional shape engineered, interfacial gelation of reduced graphene oxide for high rate, large capacity supercapacitors*. Adv Mater, [online]. 2014, vol. 26, issue 4, pp. 615-9, 505. Availble from: 10.1002/adma.201303503.

[38] Feng X., Chen W. and Yan L., *Reduced graphene oxide hydrogel film with a continuous ion transport network for supercapacitors*. Nanoscale, [online]. 2015, vol. 7, issue 8, pp. 3712-3718. Availble from: 10.1039/C4NR06897A.

[39] Moussa M., Zhao Z., El-Kady M. F., Liu H., Michelmore A., Kawashima N., Majewski P. and Ma J., *Free-standing composite hydrogel films for superior volumetric capacitance*. Journal of Materials Chemistry A, [online]. 2015, vol. 3, issue 30, pp. 15668-15674. Availble from: 10.1039/C5TA03113C.

[40] Tang Q., Sun M., Yu S. and Wang G., *Preparation and supercapacitance performance of manganese oxide nanosheets/graphene/carbon nanotubes ternary composite film*. Electrochim. Acta, [online]. 2014, vol. 125, issue pp. 488-496. Availble from: 10.1016/j.electacta.2014.01.139.

[41] Jiang J., Li Y., Liu J., Huang X., Yuan C. and Lou X. W., *Recent advances in metal oxide-based electrode architecture design for electrochemical energy*

storage. Adv Mater, [online]. 2012, vol. 24, issue 38, pp. 5166-80. Availble from: 10.1002/adma.201202146.

[42] Peng L., Peng X., Liu B., Wu C., Xie Y. and Yu G., *Ultrathin two-dimensional MnO2/graphene hybrid nanostructures for high-performance, flexible planar supercapacitors*. Nano Lett., [online]. 2013, vol. 13, issue 5, pp. 2151-7. Availble from: 10.1021/nl400600x.

[43] Tao J., Liu N., Ma W., Ding L., Li L., Su J. and Gao Y., *Solid-state high performance flexible supercapacitors based on polypyrrole-MnO2-carbon fiber hybrid structure*. Sci Rep, [online]. 2013, vol. 3, issue pp. 2286. Availble from: 10.1038/srep02286.

[44] Gao H. and Lian K., *Proton-conducting polymer electrolytes and their applications in solid supercapacitors: a review*. RSC Adv., [online]. 2014, vol. 4, issue 62, pp. 33091-33113. Availble from: 10.1039/C4RA05151C.

[45] Anothumakkool B., Torris A. T A., Bhange S. N., Unni S. M., Badiger M. V. and Kurungot S., *Design of a High Performance Thin All-Solid-State Supercapacitor Mimicking the Active Interface of Its Liquid-State Counterpart*. ACS Applied Materials & Interfaces, [online]. 2013, vol. 5, issue 24, pp. 13397-13404. Availble from: 10.1021/am404320e.

[46] Yang X., Zhang F., Zhang L., Zhang T., Huang Y. and Chen Y., *A High-Performance Graphene Oxide-Doped Ion Gel as Gel Polymer Electrolyte for All-Solid-State Supercapacitor Applications*. Advanced Functional Materials, [online]. 2013, vol. 23, issue 26, pp. 3353-3360. Availble from: 10.1002/adfm.201203556.

[47] Eigler S., Enzelberger-Heim M., Grimm S., Hofmann P., Kroener W., Geworski A., Dotzer C., Rockert M., Xiao J., Papp C., Lytken O., Steinruck H. P., Muller P. and Hirsch A., *Wet chemical synthesis of graphene*. Adv. Mater., [online]. 2013, vol. 25, issue 26, pp. 3583-7. Availble from: 10.1002/adma.201300155.

[48] Kai K., Yoshida Y., Kageyama H., Saito G., Ishigaki T., Furukawa Y. and Kawamata J., *Room-Temperature Synthesis of Manganese Oxide Monosheets*. J. Am. Chem. Soc., [online]. 2008, vol. 130, issue 47, pp. 15938-15943. Availble from: 10.1021/ja804503f.

[49] Cong H.-P., Ren X.-C., Wang P. and Yu S.-H., *Flexible graphene-polyaniline composite paper for high-performance supercapacitor*. Energy & Environmental Science, [online]. 2013, vol. 6, issue 4, pp. 1185-1191. Availble from: 10.1039/C2EE24203F.

[50] Nian Y.-R. and Teng H., *Nitric Acid Modification of Activated Carbon Electrodes for Improvement of Electrochemical Capacitance*. Journal of The Electrochemical Society, [online]. 2002, vol. 149, issue 8, pp. A1008-A1014. Availble from: 10.1149/1.1490535.

[51] Sieben J. M., Ansón-Casaos A., Montilla F., Martínez M. T. and Morallón E., *Electrochemical behaviour of different redox probes on single wall carbon nanotube buckypaper-modified electrodes*. Electrochimica Acta, [online]. 2014,

vol. 135, issue pp. 404-411. Availble from: http://dx.doi.org/10.1016/j.electacta.2014.05.016.

[52] Wang Y. G., Li H. Q. and Xia Y. Y., *Ordered Whiskerlike Polyaniline Grown on the Surface of Mesoporous Carbon and Its Electrochemical Capacitance Performance*. Advanced Materials, [online]. 2006, vol. 18, issue 19, pp. 2619-2623. Availble from: 10.1002/adma.200600445.

[53] Koo M., Park K.-I., Lee S. H., Suh M., Jeon D. Y., Choi J. W., Kang K. and Lee K. J., *Bendable Inorganic Thin-Film Battery for Fully Flexible Electronic Systems*. Nano Lett., [online]. 2012, vol. 12, issue 9, pp. 4810-4816. Availble from: 10.1021/nl302254v.

[54] Portet C., Taberna P. L., Simon P., Flahaut E. and Laberty-Robert C., *High power density electrodes for Carbon supercapacitor applications*. Electrochimica Acta, [online]. 2005, vol. 50, issue 20, pp. 4174-4181. Availble from: http://dx.doi.org/10.1016/j.electacta.2005.01.038.

[55] Wang Y., Yang X., Qiu L. and Li D., *Revisiting the capacitance of polyaniline by using graphene hydrogel films as a substrate: the importance of nano-architecturing*. Energy Environ. Sci., [online]. 2013, vol. 6, issue 2, pp. 477-481. Availble from: 10.1039/c2ee24018a.

[56] Du P., Liu H. C., Yi C., Wang K. and Gong X., *Polyaniline-Modified Oriented Graphene Hydrogel Film as the Free-Standing Electrode for Flexible Solid-State Supercapacitors*. ACS Appl. Mater. Interfaces, [online]. 2015, vol. 7, issue 43, pp. 23932-23940. Availble from: 10.1021/acsami.5b06261.

[57] Devaraj S. and Munichandraiah N., *Effect of Crystallographic Structure of MnO2 on Its Electrochemical Capacitance Properties*. J. Phys. Chem. C, [online]. 2008, vol. 112, issue 11, pp. 4406-4417. Availble from: 10.1021/jp7108785.

[58] Athouël L., Moser F., Dugas R., Crosnier O., Bélanger D. and Brousse T., *Variation of the MnO2 Birnessite Structure upon Charge/Discharge in an Electrochemical Supercapacitor Electrode in Aqueous Na2SO4 Electrolyte*. J. Phys. Chem. C, [online]. 2008, vol. 112, issue 18, pp. 7270-7277. Availble from: 10.1021/jp0773029.

[59] Gao H., Xiao F., Ching C. B. and Duan H., *High-performance asymmetric supercapacitor based on graphene hydrogel and nanostructured MnO2*. ACS Appl. Mater. Interfaces, [online]. 2012, vol. 4, issue 5, pp. 2801-10. Availble from: 10.1021/am300455d.

[60] Qu Q., Zhang P., Wang B., Chen Y., Tian S., Wu Y. and Holze R., *Electrochemical Performance of MnO2 Nanorods in Neutral Aqueous Electrolytes as a Cathode for Asymmetric Supercapacitors*. J. Phys. Chem. C, [online]. 2009, vol. 113, issue 31, pp. 14020-14027. Availble from: 10.1021/jp8113094.

[61] Dong L., Xu C., Li Y., Huang Z.-H., Kang F., Yang Q.-H. and Zhao X., *Flexible electrodes and supercapacitors for wearable energy storage: a review*

by category. J. Mater. Chem. A, [online]. 2016, vol. 4, issue 13, pp. 4659-4685. Availble from: 10.1039/c5ta10582j.

[62] Hsu Y. K., Chen Y. C., Lin Y. G., Chen L. C. and Chen K. H., *Reversible phase transformation of MnO2 nanosheets in an electrochemical capacitor investigated by in situ Raman spectroscopy*. Chem. Commun., [online]. 2011, vol. 47, issue 4, pp. 1252-4. Availble from: 10.1039/c0cc03902k.

[63] Xiong P., Ma R., Sakai N., Bai X., Li S. and Sasaki T., *Redox Active Cation Intercalation/Deintercalation in Two-Dimensional Layered MnO2 Nanostructures for High-Rate Electrochemical Energy Storage*. ACS Appl. Mater. Interfaces, [online]. 2017, vol. 9, issue 7, pp. 6282-6291. Availble from: 10.1021/acsami.6b14612.

[64] Yang S., Zhang Y., Wang L., Hong S., Xu J., Chen Y. and Li C., *Composite Thin Film by Hydrogen-Bonding Assembly of Polymer Brush and Poly(vinylpyrrolidone)*. Langmuir, [online]. 2006, vol. 22, issue 1, pp. 338-343. Availble from: 10.1021/la051581e.

[65] Jin Lee H. and Kim G. H., *Cryogenically direct-plotted alginate scaffolds consisting of micro/nano-architecture for bone tissue regeneration*. RSC Advances, [online]. 2012, vol. 2, issue 19, pp. 7578-7587. Availble from: 10.1039/C2RA20836A.

CURRICULUM VITAE

Name:	Haojie FEI
Date of birth:	9th November 1987
Place of birth:	Pinghu, Zhengjiang, China
Permanent address:	Feizhang 24, Guangcheng, Pinghu
Affiliation:	Centre of Polymer system, Faculty of Technology, Tomas Bata University in Zlin, Nám. T. G. Masaryka 5555, 760 01 Zlín
Telephone:	(+420) 773176408
E-mail:	haojie@utb.cz
Education:	2014 – to date Tomas Bata University in Zlin, Faculty of Technology, Ph.D. studies in Chemistry and Materials Technology, Specialization: Technology of Macromolecular Compounds 2010 – 2013 East China University of Science and Technology, Shanghai (China), Master`s degree in Materials Science and Engineering.  2006 – 2010 Zhejiang University of Science and Technology, Hangzhou (China), Bachelor`s degree in Materials Science and Engineering

Projects:

IGA/FT/2014/015 Cellulose based Composites for Biomedical Applications (Member)

IGA/CPS/2015/008 Bacterial Cellulose based hydrogel electrolyte: A novel supercapacitor material. (Applicant)

IGA/CPS/2016/003 In situ polymerization of poly (ethylene glycol) diacrylate based hydrogel electrolyte in flexible supercapacitors. (Applicant)

KONTAKT-II LH14273, Czech-chinese research project (Research member)

NPU I (LO1504) project, centre of polymer systems plus, TBU in Zlin (Research member)

List of publications

1 Fei, H.; Saha, N.; Kazantseva, N.; Moucka, R.; Cheng, Q.; Saha, P., A Highly Flexible Supercapacitor Based on MnO_2/RGO Nanosheets and Bacterial Cellulose-Filled Gel Electrolyte. Materials 2017, 10 (11), 1251.

2 Fei, H.; Saha N.; Kazantseva N.; Babkova T.; Machovsky M.; Wang G.; Bao H.; Saha P. Polyaniline/Reduced Graphene Oxide Hydrogel Film with Attached Graphite Current Collector for Flexible Supercapacitors. Journal of Materials Science: Materials in Electronics (accepted).

Conference proceedings cited in Web of Science/Scopus

1 Fei, H.; Saha, N.; Kazantseva, N.; Wang, G. C.; Bao, H.; Saha, P., A strong and sticky hydrogel electrolyte for flexible supercapacitors. In Proceedings of the Regional Conference Graz 2015 - Polymer Processing Society PPS: Conference Papers, Holzer, C. H.; Payer, M., Eds. Amer Inst Physics: Melville, 2016; Vol. 1779. ISBN: 978-0-7354-1441-9

2 Fei, H.; Saha, N.; Zandraa, O.; Moučka, R.; Kazantseva, N.; Wang, G.; Bao, H.; Saha, P. In situ preparation of bacterial cellulose reinforced hydrogel electrolyte for flexible supercapacitors, NANOCON 2016 - Conference

Proceedings, 8th International Conference on Nanomaterials - Research and Application, 2016; pp 583-587.ISBN: 978-80-87294-71-0

3 Shah, R.; Vyroubal, R.; **Fei, H. J.**; Saha, N.; Kitano, T.; Saha, P., Preparation of Bacterial Cellulose Based Hydrogels and Their Viscoelastic Behavior. In Novel Trends in Rheology Vi, Zatloukal, M., Ed. Amer Inst Physics: Melville, 2015; Vol. 1662. ISBN: 978-0-7354-1306-1